

---

# Covariate-informed Representation Learning with Samplewise Optimal Identifiable Variational Autoencoders

---

Young-geun Kim<sup>1,2</sup> Ying Liu<sup>1,2</sup> Xuexin Wei<sup>3</sup>

## Abstract

Recently proposed identifiable variational autoencoder (iVAE, Khemakhem et al. (2020)) framework provides a promising approach for learning latent independent components of the data. Although the identifiability is appealing, the objective function of iVAE does not enforce the inverse relation between encoders and decoders. Without the inverse relation, representations from the encoder in iVAE may not reconstruct observations, i.e., representations lose information in observations. To overcome this limitation, we develop a new approach, covariate-informed identifiable VAE (CI-iVAE). Different from previous iVAE implementations, our method critically leverages the posterior distribution of latent variables conditioned only on observations. In doing so, the objective function enforces the inverse relation, and learned representation contains more information of observations. Furthermore, CI-iVAE extends the original iVAE objective function to a larger class and finds the optimal one among them, thus providing a better fit to the data. Theoretically, our method has tighter evidence lower bounds (ELBOs) than the original iVAE. We demonstrate that our approach can more reliably learn features of various synthetic datasets, two benchmark image datasets (EMNIST and Fashion MNIST), and a large-scale brain imaging dataset for adolescent mental health research.

ture generating observations, to cluster observations by semantic meaning, and to detect anomalous patterns (Bengio et al., 2013; LeCun et al., 2015). An important application is scientific exploratory analysis, such as to learn the representation of high-dimensional genetic/brain imaging data associated with phenotypes (Liu et al., 2009; Pearson et al., 2015; Sui et al., 2013; Way et al., 2020).

Many variations of independent component analysis (ICA, Hyvärinen (2013)) and autoencoders (AE, Bengio et al. (2007)) have been proposed for representations. ICA assumes that observations are generated by mapping linearly independent components (ICs) through linear mixing functions and learns the ICs and mixing functions. AE extracts representations with encoders (often via nonlinear neural networks), and representations can reconstruct observations with decoders. Variational autoencoders (VAE, Kingma & Welling (2014)) have been proposed to learn representations and generate samples, but the likelihood models are not *identifiable*, i.e., two different parameters can provide the same likelihood (Locatello et al., 2019; Khemakhem et al., 2020).

For the purpose of obtaining more interpretable representations with nonlinear models, Khemakhem et al. defined *identifiability* of deep generative models when covariates are available in addition to observations and proposed identifiable VAE (iVAE). A generative model is called identifiable if the distribution of its output is identified by its parameters. With identifiable likelihood models, iVAE estimates true ICs and nonlinear mixing functions by maximizing the evidence lower bound (ELBO). However, the ELBO of iVAE does not enforce the inverse relation between encoders and decoders (a detailed review on the importance of the inverse relation and AE-based representation learning methods are provided in Section 2). Without the inverse relation, representations from encoders in iVAE may not reconstruct observations.

To overcome the limitation of iVAE, we propose a new method, the Covariate-Informed Identifiable VAE (CI-iVAE). Our method leverages encoders in addition to the original posterior distribution considered in the previous iVAE to derive alternative ELBOs. In doing so, our objective function encourages the inverse relation between encoders and decoders while maximizing the likelihood of

## 1. Introduction

Representation learning is the task of identifying low-dimensional latent codes that can be used to infer the struc-

---

\*Equal contribution <sup>1</sup>Department of Biostatistics, Mailman school of public health, Columbia University, New York, United States <sup>2</sup>Division of Mental Health Data Science, New York State Psychiatry Institute <sup>3</sup>Department of Neuroscience and Department of Psychology, The University of Texas at Austin. Correspondence to: Ying Liu <Ying.Liu@nyspi.columbia.edu>.

identifiable models. CI-iVAE extends the iVAE objective function to a larger class and finds the samplewise optimal one among them, so it provides a better account of the data. We show that, theoretically, the proposed method has tighter ELBOs than the original iVAE under mild conditions.

We apply our method and iVAE to a brain imaging dataset, Adolescent Brain Cognitive Development (ABCD) study.<sup>1</sup> Our experiment on the ABCD dataset is the first to learn ICs from brain imaging with identifiable neural networks. Our method successfully learns representations from brain imaging data associated with the characteristics of subjects while iVAE does not.

Our contributions can be summarized as follows:

- We propose CI-iVAE to learn better representations than iVAE by modifying the ELBO of iVAE to enforce the inverse relation between encoders and decoders.
- We derive that the proposed method has strictly tighter ELBOs than iVAE when the signal-to-noise ratio between encoder and posterior distribution in the original iVAE are large (Theorem 1).
- Experimental results on various simulations and real datasets demonstrate that our methods learn better representations than existing methods in terms of extracting covariates-associated information in observations. Our work is the first to learn independent components of brain imaging with identifiable generative models.

All proofs of theoretical results are provided in Appendix A. Implementation details are provided in Appendix B.

## 2. Related Prior Work

In this section, we review related works on representation learning. We first review methods using only observations and then describe their extensions to cases where covariates are available in addition to observations.

The encoder of AE and its variations have been recognized as effective nonlinear feature extractors (Vincent et al., 2008; Rifai et al., 2011; Zong et al., 2018). Their effectiveness comes from the reconstruction error enforcing the inverse relation between encoders and decoders. The reconstruction error is a distance between observations and their reconstruction results with extracted representations and decoders. For example, generative autoencoders such as VAE and Wasserstein autoencoders (WAE, Tolstikhin et al. (2018)) use reconstruction errors with penalty terms as objective functions. Penalty terms in VAE and WAE, respectively, are to compute the ELBO (Bishop, 2006) and is to approximate Wasserstein

<sup>1</sup>The ABCD dataset can be found at <https://abcdstudy.org>, held in the NIMH Data Archive (NDA).

distance (Vaserstein, 1969). Other examples in anomaly detection literature, Zenati et al. and Schlegl et al. introduced encoders to generative adversarial networks (Goodfellow et al., 2014) and enforced to reconstruct observations with encoders and generators to learn better representations.

In the cases where covariates are available, many conditional generative models have been proposed to incorporate covariates in generators in addition to latent variables. In conditional VAE (Sohn et al., 2015) and conditional adversarial autoencoders (Makhzani et al., 2015), covariates are feed-forwarded by both encoder and decoder. Auxiliary classifiers for covariates are usually applied to learn representations that can generate better results (Kameoka et al., 2018; Zhao et al., 2018). The aforementioned methods have shown prominent generation results, but their models can learn the distribution of observations with many different prior distributions of latent variables, i.e., they are not *identifiable* (Khemakhem et al., 2020). Another limitation is that their encoders require covariates in addition to observations. In contrast, our method learns representations with identifiable generative models, and our encoders do not require covariates to extract representations.

Inspired by the iVAE framework, recently, some identifiable generative models have been proposed. Zhou & Wei proposed Poisson identifiable VAE (pi-VAE) to extend the data generation structure of iVAE from continuous observation noise cases to Poisson, but, as in iVAE, the ELBO in pi-VAE does not enforce the inverse relation between encoders and decoders. Sorrenson et al. proposed general incompressible-flow networks (GIN), volume-preserving invertible neural networks, and modified network architectures of iVAE to satisfy the inverse relation. However, due to the volume-preserving invertibility condition, the dimension of latent variables is the same as that of observations. The number of network parameters is enormous, and the depth of networks is limited when observations are high-dimensional.

## 3. Proposed Method

### 3.1. Preliminaries

#### 3.1.1. BASIC NOTATIONS AND ASSUMPTIONS

We denote observations, covariates, and latent variables by  $X \in \mathbb{R}^{d_x}$ ,  $U \in \mathbb{R}^{d_u}$ , and  $Z \in \mathbb{R}^{d_z}$ , respectively. The dimension of latent variables is lower than that of observations, i.e.,  $d_z < d_x$ . For a given random variable (e.g.,  $Z$ ), its realization and probability density function (p.d.f.) is denoted by small letter (e.g.,  $z$ ) and  $p$  (e.g.,  $p(z)$ ), respectively. For any random variables  $A$  and  $B$ , the conditional distribution of  $A$  given  $B$  is denoted by  $p(a|b)$ . We write the parameters (e.g.,  $\theta$ ) for model distributions in subscripts (e.g.,  $p_\theta(x, z)$ ). For distributions in variational inference, we use  $q$  instead of  $p$  (e.g.,  $q_\phi(z|x, u)$ ). The expectation

operation and Kullback-Leibler divergence are denoted by  $\mathbb{E}$  and  $\mathcal{D}_{\text{KL}}$ , respectively.

### 3.1.2. NONLINEAR INDEPENDENT COMPONENT ANALYSIS

We provide a formulation of nonlinear ICA (Hyvärinen & Oja, 2000; Jutten et al., 2010). The nonlinear ICA assumes the following data generation structure:

$$\begin{cases} Z_i \perp\!\!\!\perp Z_j \text{ for any two different } i, j = 1, \dots, d_Z \\ X = f_0(Z) \end{cases} \quad (1)$$

where  $Z_i$  and  $Z_j$  are  $i$ -th and  $j$ -th attributes of  $Z$ , respectively. Here, the  $Z$  is called the *independent component* (or *source*), and  $f_0$  is called the *mixing function*. The difference from (linear) ICA is that the mixing function  $f_0$  is invertible and nonlinear.

The goal of nonlinear ICA is to learn representations by finding the inverse of the mixing function  $f_0^{-1}$ . However, with only observations, the problem of finding latent variables and nonlinear functions satisfying Equation (1) can have infinitely many solutions (Hyvärinen & Pajunen, 1999). Hyvärinen & Morioka provided the first identifiable nonlinear ICA, assuming that observations are time series and ICs follow conditionally factorial exponential family distributions parameterized by time segments, a covariate. Hyvärinen et al. provided more general results on identifiable nonlinear ICA, and Khemakhem et al. extended these results to data generation structures with observation noise by founding the identifiability of deep generative models.

### 3.1.3. IDENTIFIABLE VARIATIONAL AUTOENCODERS

The iVAE framework provides an appealing approach for learning latent ICs and nonlinear mixing functions. The iVAE models the mixing function with neural networks, a flexible nonlinear model, and its generation process is *identifiable* where the consistency of estimated ICs and mixing functions are guaranteed under certain conditions. We first formulate the iVAE framework and then review the identifiability of generative models. Key components of iVAE include label prior, decoder, and posterior networks. The label prior and decoder, respectively, models the conditional distribution of latent variables given covariates,  $p(z|u)$ , and observations given latent variables,  $p(x|z)$ . The posterior networks models the posterior distribution (or inference model) of the latent variables,  $q(z|x, u)$ .

An essential condition on the label prior to identifiability is the conditionally factorial exponential family distribution assumption. The label prior is denoted by  $p_{T,\lambda}(z|u)$  and can be expressed as  $p_{T,\lambda}(z|u) = \prod_{i=1}^{d_Z} p_{T_i,\lambda_i}(z_i|u)$  where  $p_{T_i,\lambda_i}(z_i|u) = \exp(\lambda_i(u) \cdot T_i(z_i) - A(u) + B(z_i))$  is the exponential family distribution with parameters  $\lambda_i(u)$ , sufficient statistics  $T_i(z_i)$ , and known functions  $A$  and  $B$ .

Table 1. A summary of various autoencoders according to identifiability and inverse relation between encoders and decoders. Our method modifies the ELBO of iVAE to enforce the inverse relation so that it can extract representations with the inverse of the mixing function.

METHOD	IDENTIFIABILITY	INVERSE RELATION BETWEEN ENCODER AND DECODER
VAE	✗	✓
iVAE	✓	✗
Ours	✓	✓

We denote  $T := (T_1, \dots, T_{d_Z})$  and  $\lambda := (\lambda_1, \dots, \lambda_{d_Z})$ . The decoder is denoted by  $p_f(x|z) := p(\epsilon = x - f(z))$  where  $f$  is the modeled mixing function and  $p(\epsilon)$  is the p.d.f. of noise variables  $\mathcal{E}$ . With label prior and decoder, the data generation process can be expressed as  $p_\theta(x, z|u) := p_f(x|z)p_{T,\lambda}(z|u)$  where  $\theta = (f, T, \lambda)$  is all the parameters for the data generation process. The posterior model is denoted by  $q_\phi(z|x, u)$  and the encoder can be estimated by  $q_\phi(z|x) = \int q_\phi(z|x, u)p(u|x)du$ . The role of  $q_\phi(z|x, u)$  is to model posterior distributions of the label prior with observations to derive ELBO. The ELBO in iVAE is with respect to (w.r.t.) the conditional log-likelihood of observations given covariates,  $p_\theta(x|u)$ , and can be expressed as

$$\mathbb{E}_{q_\phi(z|x, u)} \log p_f(x|z) - \mathcal{D}_{\text{KL}}(q_\phi(z|x, u) || p_{T,\lambda}(z|u)). \quad (2)$$

In the implementation, iVAE models  $p_{T,\lambda}(z|u)$  and  $q_\phi(z|x, u)$  with Gaussian distributions.

A generative model is called *identifiable* if the distribution of its output is identified by its parameters.

**Definition 1.** (Identifiability, Khemakhem et al. (2020)) *A generative model  $p_\theta(x, z|u)$  is called identifiable if the following holds: For any  $\theta = (f, T, \lambda)$  and  $\tilde{\theta} = (\tilde{f}, \tilde{T}, \tilde{\lambda})$ ,  $p_\theta(x|u) = p_{\tilde{\theta}}(x|u)$  implies  $\theta \sim \tilde{\theta}$ . Here,  $\theta \sim \tilde{\theta}$  is defined as  $T(f^{-1}(x)) = \tilde{T}(\tilde{f}^{-1}(x))$  with probability 1 up to a invertible affine transformation.*

Under the identifiability, maximizing likelihood implies learning the true mixing function and ICs in Equation (1). Khemakhem et al. showed that the identifiability holds if  $f$  is injective,  $\lambda$  can make invertible matrix  $(\lambda(u_1) - \lambda(u_0), \dots, \lambda(u_{nk}) - \lambda(u_0))$  with some  $nk + 1$  distinct  $u_0, \dots, u_{nk}$ ,<sup>2</sup> and some mild conditions hold.

## 3.2. Motivation

Our goal is to learn  $f_0^{-1}(X)$  with nonlinear identifiable generative models and to use it as representations. The  $f_0^{-1}(X)$

<sup>2</sup>Recently, the paper at <https://openreview.net/forum?id=AMpki9kp8Cn> weakened this assumption and provided other conditions for the identifiability.

is a novel representation since it contains all the information in observations and is the ICs, true latent variables when the observation noise is zero.

The identifiability of the likelihood model and the inverse relation between encoders and decoders are two essential conditions to learn  $f_0^{-1}$ . The decoder  $p_f(x|z)$  from identifiable models is close to the true mixing function  $f_0$  when the likelihood is maximized well, but the identifiability alone does not guarantee any properties of encoder  $q_\phi(z|x)$ . If the inverse relation between  $q_\phi(z|x)$  and  $p_f(x|z)$  pair holds in addition to identifiability, the encoder is guaranteed to be close to the inverse of the mixing function,  $f_0^{-1}$ , when the likelihood is maximized well. Most of the AE-based methods enforce the inverse relation with reconstruction errors in objective functions, but their likelihood models are not identifiable. In contrast, iVAE uses identifiable likelihood models, but its objective function does not enforce the inverse relation. For details, VAE uses the reconstruction error (or reconstruction probability),  $\mathbb{E}_{q_\phi(z|x)} \log p_f(x|z)$ , in its ELBO to enforce the inverse relation. In iVAE, though  $q_\phi(z|x)$  and  $p_f(x|z)$  are called by autoencoders (AE) to inherit the terminology of VAE, Equation (2) does not contain the reconstruction error, so the inverse relation is not enforced. It is a limitation of representations from iVAE.

We evaluate various autoencoders whether the identifiability and the inverse relation between encoders and decoders for learning  $f_0^{-1}$  are satisfied in Table 1. Our method modifies the ELBO of iVAE to enforce the inverse relation so that it can extract representations with the inverse of the mixing function. GIN is the only existing work that fulfills the two conditions and can conduct this task, but the number of network parameters is enormous, and the depth of networks is limited when observations are high-dimensional.

Our method learns  $f_0^{-1}$  by incorporating  $q_\phi(z|x)$  in ELBO to learn identifiable models. For a motivating example, we can learn  $f_0^{-1}$  by maximizing other ELBO,

$$\mathbb{E}_{q_\phi(z|x)} \log p_f(x|z) - \mathcal{D}_{\text{KL}}(q_\phi(z|x) || p_{T,\lambda}(z|u)), \quad (3)$$

which is derived by replacing  $q_\phi(z|x, u)$  in Equation (2) with  $q_\phi(z|x)$ . We name Equations (2) and (3) by ELBO with  $q_\phi(z|x, u)$  and with  $q_\phi(z|x)$ , respectively. Note that the ELBO with  $q_\phi(z|x)$  encourages to learn  $f_0^{-1}$  when  $p_\theta(x, z|u)$  is identifiable. For simplicity, let assume that the ELBO with  $q_\phi(z|x)$  is maximized well so that  $f$  and  $p_{T,\lambda}(z|u)$  are close to  $f_0$  and the distribution of ICs, respectively. In this case, the first term (reconstruction error) directly enforces the inverse relation between  $q_\phi(z|x)$  and  $p_{f_0}(x|z)$  and the second term indirectly enforces it by matching  $q_\phi(z|x)$  and the distribution of ICs which are  $f_0^{-1}(x)$  when observation noise is small (or covariates are informative).

The ELBO with  $q_\phi(z|x)$  allows to learn  $f_0^{-1}$ , but it may be

less tight lower bound of  $\log p_\theta(x|u)$  than the ELBO with  $q_\phi(z|x, u)$  since the  $q_\phi(z|x, u)$  is more flexible by incorporating covariates. Thus, we need to find a good balance between the sharpness of lower bounds to estimate  $f_0$  and the enforcement of the inverse relation between encoders and decoders to learn  $f_0^{-1}$  with estimated  $f_0$ . In the next section, we provide our method leveraging them by considering a set of ELBOs, including ELBOs with  $q_\phi(z|x)$  and  $q_\phi(z|x, u)$ .

### 3.3. Covariate-informed Identifiable VAE

In this section, we provide our method, covariate-informed iVAE, to learn representations extracted with the inverse of the mixing function  $f_0^{-1}$ . We use the same architecture of iVAE described in Section 3.1.3 to inherit the identifiability of the likelihood model, but we target different objective functions to enforce the inverse relation between encoders and decoders while maximizing the sharper lower bound of the conditional log-likelihood.

As described in Section 3.2, for a given identifiable  $p_\theta(x, z|u)$ , two properties of the objective function are required to learn  $f_0^{-1}$ : (i) it assists in maximizing the log-likelihood to estimate  $f_0$  and ICs, and (ii) it enforces the inverse relation between encoders and decoders to learn  $f_0^{-1}$  with estimated  $f_0$ . The ELBO with  $q_\phi(z|x, u)$  (Equation (2)) is better at (i), and the ELBO with  $q_\phi(z|x)$  (Equation (3)) is better at (ii), so we consider mixtures of distributions by encoders  $q_\phi(z|x)$  and the posterior in the original iVAE,  $q_\phi(z|x, u)$ ,

$$\{\alpha q_\phi(z|x) + (1 - \alpha) q_\phi(z|x, u) | \alpha \in [0, 1]\}, \quad (4)$$

to achieve (ii) while enjoying sharper lower bounds of conditional log-likelihood for (i).

We first formulate a set of ELBOs using Equation (4) and then provide our method. The role of  $q_\phi(z|x, u)$  in the original iVAE is to compute a lower bound of log-likelihood, the ELBO with  $q_\phi(z|x, u)$ , and any element in Equation (4) can serve this role.

**Proposition 1.** For any sample  $(x, u)$ ,  $\theta = (f, T, \lambda)$ ,  $\phi$ , and  $\alpha \in [0, 1]$ ,  $ELBO_{\theta, \phi}(\alpha; x, u)$  defined as

$$\begin{aligned} & \mathbb{E}_{\alpha q_\phi(z|x) + (1-\alpha) q_\phi(z|x, u)} \log p_f(x|z) \\ & - \mathcal{D}_{\text{KL}}(\alpha q_\phi(z|x) + (1 - \alpha) q_\phi(z|x, u) || p_{T,\lambda}(z|u)) \end{aligned}$$

is a lower bound of  $\log p_\theta(x|u)$ .

The Proposition 1 can be derived by conducting variational inference with  $\alpha q_\phi(z|x) + (1 - \alpha) q_\phi(z|x, u)$ . A set of ELBOs,  $\{ELBO_{\theta, \phi}(\alpha; x, u) | \alpha \in [0, 1]\}$  is a continuum of ELBOs whose endpoints are ELBOs with  $q_\phi(z|x, u)$  and with  $q_\phi(z|x)$ .

**Algorithm 1** Finding Samplewise Optimal iVAEs

**Input:** A sample  $(x, u)$ , encoder networks  $q_\phi(z|x)$ , label prior networks  $p_{T,\lambda}(z|u)$ , decoder networks  $p_f$ , the number of sample for Monte Carlo approximation  $M$ , a finite set of real numbers  $A \subset [0, 1]$

**Output:** The  $\alpha^*$  to inform the optimal iVAE for the sample  $(x, u)$

- 1: Sample  $z_m^{\text{enc}}$  from  $q_\phi(z|x)$  for  $m = 1, \dots, M$
- 2: Sample  $z_m^{\text{post}}$  from  $q(z|x, u)$  for  $m = 1, \dots, M$
- 3:  $\text{ELBO}_{\theta,\phi}(0; x, u) \leftarrow \log p_f(x|z_1^{\text{post}}) - \mathcal{D}_{\text{KL}}(q(z|x, u)||p_{T,\lambda}(z|u))$
- 4:  $\text{ELBO}_{\theta,\phi}(1; x, u) \leftarrow \log p_f(x_b|z_1^{\text{enc}}) - \mathcal{D}_{\text{KL}}(q_\phi(z|x)||p_{T,\lambda}(z|u))$
- 5:  $\mathcal{D}_{\text{Skew}}^{1-\alpha}(q_\phi(z|x)||q(z|x, u)) \leftarrow M^{-1} \sum_{m=1}^M \log q_\phi(z_m^{\text{enc}}|x) / (\alpha q_\phi(z_m^{\text{enc}}|x) + (1-\alpha)q(z_m^{\text{enc}}|x, u))$  for  $\alpha \in A$
- 6:  $\mathcal{D}_{\text{Skew}}^\alpha(q(z|x, u)||q_\phi(z|x)) \leftarrow M^{-1} \sum_{m=1}^M \log q(z_m^{\text{post}}|x, u) / (\alpha q_\phi(z_m^{\text{post}}|x) + (1-\alpha)q(z_m^{\text{post}}|x, u))$  for  $\alpha \in A$
- 7:  $\text{ELBO}_{\theta,\phi}(\alpha; x, u) \leftarrow \alpha \text{ELBO}_{\theta,\phi}(1; x, u) + (1-\alpha) \text{ELBO}_{\theta,\phi}(0; x, u) - \alpha \mathcal{D}_{\text{Skew}}^{1-\alpha}(q_\phi(z|x)||q(z|x, u)) - (1-\alpha) \mathcal{D}_{\text{Skew}}^\alpha(q(z|x, u)||q_\phi(z|x))$  for  $\alpha \in A$
- 8:  $\alpha^*(x, u) = \arg \max_{\alpha \in A} \text{ELBO}_{\theta,\phi}(\alpha; x, u)$

**Algorithm 2** Training CI-iVAE

**Input:** Training samples  $\{(x_i, u_i)\}_{i=1}^n$ , encoder networks  $q_\phi$ , label prior networks  $p_{T,\lambda}$ , decoder networks  $p_f$ , batch size  $B$ , the number of sample for Monte Carlo approximation  $M$ , a finite set of real numbers  $A \subset [0, 1]$

**Output:** CI-iVAE with  $(T^*, \lambda^*, f^*)$  and encoder networks with  $\phi^*$

- 1: Initialize  $(T, \lambda, \phi, f)$
- 2: **While**  $(T, \lambda, \phi, f)$  did not converge **Do**
- 3: Sample  $\{(x_{i(b)}, u_{i(b)})\}_{b=1}^B$  from training samples
- 4: Calculate  $\alpha^*(x_{i(b)}, u_{i(b)})$  with Algorithm 1
- 5: Update  $(T, \lambda, \phi, f)$  by ascending

$$B^{-1} \sum_{b=1}^B \text{ELBO}_{\theta,\phi}(\alpha^*(x_{i(b)}, u_{i(b)}); x_{i(b)}, u_{i(b)})$$

- 6:  $(T^*, \lambda^*, \phi^*, f^*) \leftarrow (T, \lambda, \phi, f)$

We now present the covariate-informed iVAE (CI-iVAE). For a given identifiable  $p_\theta(x, z|u)$ , different from VAE using  $q_\phi(z|x)$  for variational inference, the CI-iVAE uses covariates to find the optimal distribution in Equation (4) and utilizes it for deriving ELBO. The optimal mixing proportion informed by covariates is denoted by  $\alpha^*(x, u) := \arg \max_{\alpha \in [0,1]} \text{ELBO}_{\theta,\phi}(\alpha; x, u)$  and it defines the samplewise optimal iVAE whose ELBO is the sharpest. In this way, our method uses sharper lower bounds than the existing iVAE method for all samples and enforces the inverse relation between encoders and decoders as well, yielding representations closer to  $f_0^{-1}(x)$ . The objective function of CI-iVAE is

$$\text{ELBO}_{\theta,\phi}(\alpha^*(x, u); x, u). \quad (5)$$

Furthermore, we derive that the difference between our optimal ELBO and the ELBO of existing iVAE is significant in Theorem 1 in the next section.

Though the CI-iVAE allows learning better representations, numerical approximation for  $\alpha^*(x, u)$  in Equation (5) may lead to burdensome computational costs. To overcome this technical obstacle, we provide an alternative expression of our objective function that allows us to approximate  $\alpha^*(x, u)$  within twice the computation time of the ELBO of the existing iVAE.

**Proposition 2.** For any sample  $(x, u)$ ,  $\theta = (f, T, \lambda)$ ,  $\phi$ , and  $\alpha \in [0, 1]$ ,  $\text{ELBO}_{\theta,\phi}(\alpha; x, u)$  can be expressed as

$$\alpha \text{ELBO}_{\theta,\phi}(1; x, u) + (1-\alpha) \text{ELBO}_{\theta,\phi}(0; x, u) + \alpha \mathcal{D}_{\text{Skew}}^{1-\alpha}(q_\phi(z|x)||q_\phi(z|x, u)) + (1-\alpha) \mathcal{D}_{\text{Skew}}^\alpha(q_\phi(z|x, u)||q_\phi(z|x)),$$

where  $\mathcal{D}_{\text{Skew}}^\alpha$  is the skew divergence defined as  $\mathcal{D}_{\text{Skew}}^\alpha(p||q) := \mathcal{D}_{\text{KL}}(p||((1-\alpha)p + \alpha q))$  (Lin, 1991).

Details on finding samplewise optimal iVAEs with Proposition 2 and using optimal iVAEs to maximize Equation (5) are described in Algorithms 1<sup>3</sup> and 2, respectively. The main bottleneck is on computing  $\text{ELBO}_{\theta,\phi}(0; x, u)$ ,  $\text{ELBO}_{\theta,\phi}(1; x, u)$ , and conditional means and standard deviations of the label prior and encoder distributions, which requires roughly twice the computation time of the ELBO of iVAE. With Proposition 2 and reparametrization trick, for any  $\alpha$ , the remaining process to compute  $\text{ELBO}_{\theta,\phi}(\alpha; x, u)$  is completed in a short time.

### 3.4. Theoretical Properties of CI-iVAE

In this section, we derive the concavity and sharpness of proposed ELBOs. The concavity implies that the approximation error for  $\alpha^*(x, u)$  is small. For the sharpness, our method uses a sharper lower bound of conditional log-likelihood than the existing iVAE with positive margins.

We first show the concavity of the proposed ELBO and a necessary and sufficient condition for the linearity.

<sup>3</sup>As in pi-VAE (Zhou & Wei, 2020), we model Gaussian distributions for label prior  $p_{T,\lambda}(z|u)$  and encoder  $q_\phi(z|x)$ , and assume  $q(z|x, u) \propto q_\phi(z|x)p_{T,\lambda}(z|u)$ .

**Proposition 3.** For any sample  $(x, u)$  and  $\alpha \in [0, 1]$ ,  $ELBO_{\theta, \phi}(\alpha; x, u)$  is concave w.r.t.  $\alpha$ . It is linear if and only if  $q_{\phi}(z|x) = q_{\phi}(z|x, u)$  for all  $z$ .

Note that the first two terms in Proposition 2 are linear w.r.t.  $\alpha$ , and the last two terms are zero if and only if  $q_{\phi}(z|x) = q_{\phi}(z|x, u)$  for all  $z$ . That is, divergences between two endpoints in Equation (4) induce the concavity. With the concavity, the numerical approximation error for  $\alpha^*(x, u)$  by grid search can be small.

Next, we show that our method uses sharper lower bounds than the existing iVAE. Let  $\Delta_{1-0}(x, u) := ELBO_{\theta, \phi}(1; x, u) - ELBO_{\theta, \phi}(0; x, u)$  and

$$SNR(g) := \frac{(\mathbb{E}_{q_{\phi}(z|x)}g(z) - \mathbb{E}_{q_{\phi}(z|x, u)}g(z))^2}{\max(Var_{q_{\phi}(z|x)}g(z), Var_{q_{\phi}(z|x, u)}g(z))}. \quad (6)$$

Here,  $SNR(g)$  is the signal-to-noise ratio between  $q_{\phi}(z|x)$  and  $q_{\phi}(z|x, u)$  w.r.t.  $g$ .

**Theorem 1.** For any sample  $(x, u)$ ,  $\theta = (f, T, \lambda)$ ,  $\phi$ , and  $\epsilon > 0$ , if there is a function  $g : \mathcal{Z} \rightarrow \mathbb{R}$  satisfying  $SNR(g) \geq 1/\epsilon$  and  $|\Delta_{1-0}(x, u)| \leq -\log \epsilon + O(\epsilon \log \epsilon)$ , then

$$\begin{aligned} & \sup_{\alpha \in [0, 1]} ELBO_{\theta, \phi}(\alpha; x, u) - ELBO_{\theta, \phi}(0; x, u) \\ & \geq \frac{-1 + \sqrt{1 + 4\epsilon}}{2} |\Delta_{1-0}(x, u)| + o(|\Delta_{1-0}(x, u)|) + O(\epsilon \log \epsilon) \\ & \text{as } |\Delta_{1-0}(x, u)| \rightarrow \infty \text{ and } \epsilon \rightarrow 0^+. \end{aligned}$$

That is, if  $q_{\phi}(z|x)$  and  $q_{\phi}(z|x, u)$  are different so that  $SNR(g)$  is large enough for some  $g$ , then our bound is sharper than that of iVAE with positive margins. Note that our bound is sharper even Equation (2) is much larger than (3), i.e.,  $|\Delta_{1-0}(x, u)|$  is large.

We provide an approximation formula for  $\alpha^*$ ,

$$\alpha_{\text{approx}}^*(\epsilon, \Delta_{1-0}(x, u)) := \frac{1 - \sqrt{1 + 4\epsilon}}{2} + \frac{\sqrt{1 + 4\epsilon}}{1 + e^{-\sqrt{1 + 4\epsilon} \Delta_{1-0}(x, u)}}. \quad (7)$$

The  $\alpha_{\text{approx}}^*$  is the maximizer of a lower bound of  $ELBO_{\theta, \phi}(\alpha; x, u) - ELBO_{\theta, \phi}(0; x, u)$  in Lemma 2 in Appendix A. Details on  $\alpha_{\text{approx}}^*$  are provided in Lemma 4 in Appendix A. Since the lower bound evaluated at  $\alpha = \alpha_{\text{approx}}^*$  is the RHS in Theorem 1, the  $\alpha_{\text{approx}}^*$  can be used to approximate  $\alpha^*$ . In the simulation study in Table 7 in Appendix B.2, calculated values by this formula are similar to  $\alpha^*$  from Algorithm 1, which supports the validity of our theory.

## 4. Experiments

We have validated and applied our method on synthetic, extended MNIST (EMNIST, Cohen et al. (2017)), Fashion-MNIST (Xiao et al., 2017), and ABCD (Jernigan et al., 2018) datasets. For CI-iVAE, we implement two versions: (i) CI-iVAE with  $\alpha^* = 1$  for all samples and (ii) CI-iVAE

Table 2. Means of evaluation metrics with standard errors from various methods on the sine latent structure. The number of repeats is 20. Results for all latent structures are provided in Table 6 in Appendix B.2.

METHOD	EVALUATION METRIC	
	MSE ( $\downarrow$ )	LOG-LIKELIHOOD ( $\uparrow$ )
iVAE	0.0368 (0.0049)	-131.8387 (1.7467)
CI-iVAE WITH $\alpha^* = 1$ FOR ALL SAMPLES	0.0083 (0.0003)	-112.9937 (0.8611)
CI-iVAE WITH SAMPLEWISE $\alpha^*$	<b>0.0072</b> (0.0002)	<b>-111.2823</b> (0.5576)

with samplewise optimal  $\alpha^*$ . (i) and (ii) use Equations (3) and (5) as objective functions, respectively, and (i) is a simplified version of (ii) without fully addressing samplewise optimal VAEs. Implementation details, including data descriptions and network architectures, are provided in Appendix B.1.

### 4.1. Simulation Study

Using synthetic datasets, we first examine the effectiveness of applying samplewise optimal VAEs by comparing three cases: 1) iVAE (is equivalent to CI-iVAE with  $\alpha^* = 0$  for all samples), 2) CI-iVAE with  $\alpha^* = 1$  for all samples, and 3) CI-iVAE with samplewise optimal  $\alpha^*$ . Both 1) and 2) are simplified versions of CI-iVAE. We use three data generation schemes and named them by shapes of the conditional expectation of latent variables given covariates: (i) sine, (ii) quadratic, and (iii) two circles.

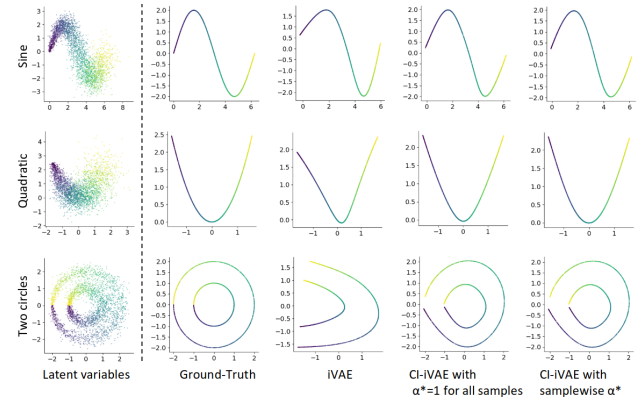


Figure 1. Visualization of latent variables in simulation study and results from various methods.

Table 2 and Figure 1 show the results from the synthetic dataset. We consider two evaluation metrics using ground-truth latent variables, MSE between true and estimated latent variables and maximized log-likelihood. The MSE is used to evaluate the learned latent structure. We first fit

linear regression models for applying affine transformations to estimated results and then calculate Euclidean distances between conditional expectations of ground-truth and estimated latent variables given covariates. The log-likelihood is used to evaluate the whole data generation scheme. All methods use the same network architectures, so the density models are the same. The log-likelihood is calculated by  $\log p_\theta(x|u) = \log \int p_f(x|z)p_{T,\lambda}(z|u)dz$  with Monte Carlo approximation and is averaged over samples.

According to Table 2, the iVAE is worse than the other two. When iVAE is compared with CI-iVAE with samplewise  $\alpha^*$ , p-values are  $4.5 \times 10^{-6}$  for MSE and  $4.0 \times 10^{-10}$  for log-likelihood. Moreover, CI-iVAE with samplewise optimal  $\alpha^*$  is better than CI-iVAE with  $\alpha^* = 1$  for all samples. The p-values are  $1.1 \times 10^{-2}$  for MSE and  $5.6 \times 10^{-2}$  for log-likelihood. That is, our sharper ELBO enhances performances on learning ground-truth ICs and mixing functions.

Visualization of latent variables and results is presented in Figure 1. The latent variables (Column 1), the ground-truth conditional expectation of latent variables given covariates (Column 2), and conditional expectations of latent prior from various methods (From columns 3 to 5) are colored by covariates. For the two circles structure, we color data-points by angles,  $U_1$ . In all latent structures, CI-iVAE with samplewise optimal  $\alpha^*$  and CI-iVAE with  $\alpha^* = 1$  for all samples are better than iVAE in recovering the conditional expectation of latent variables given covariates.

## 4.2. Applications to Real Datasets

### 4.2.1. EMNIST AND FASHION-MNIST

We compare the proposed CI-iVAE with GIN and iVAE on two benchmark image datasets: EMNIST and Fashion-MNIST. In EMNIST, observations and covariates are images of handwritten digits and digit labels, respectively. In Fashion-MNIST, observations and covariates are images of fashion items such as ankle boots, bags, and coats, and item labels, respectively.

The experimental results are presented in Table 3 and Figure 2. Generation results are provided in Figures 4, 5, and 6 in Appendix B.2. We consider the ratio of the within-cluster sum of squares (SSW) over the total sum of squares (SST) as evaluation metrics. The SSW/SST is used to measure how well representations are clustered by covariates. It is calculated with Euclidean distances between conditional expectations of latent variables for given observations.

According to Table 3, for all datasets, the iVAE that does not enforce the inverse relation between encoders and decoders is worse than our methods, CI-iVAE with  $\alpha^* = 1$  for all samples and with samplewise optimal  $\alpha^*$ . Our methods also are better than GIN in all datasets. When iVAE is compared with CI-iVAE with samplewise  $\alpha^*$ , p-values are

Table 3. Means of evaluation metrics with standard errors from various methods on EMNIST and Fashion-MNIST datasets. The number of repeats is 20.

DATASET	METHOD	SSW/SST ( $\downarrow$ )
EMNIST	GIN	.6130 (.0075)
	iVAE	.5486 (.0037)
	CI-iVAE WITH $\alpha^* = 1$ FOR ALL SAMPLES	<b>.4060</b> (.0026)
	CI-iVAE WITH SAMPLEWISE $\alpha^*$	.4117 (.0032)
FASHION-MNIST	GIN	.8503 (.0026)
	iVAE	.6157 (.0046)
	CI-iVAE WITH $\alpha^* = 1$ FOR ALL SAMPLES	<b>.4777</b> (.0024)
	CI-iVAE WITH SAMPLEWISE $\alpha^*$	.4926 (.0024)

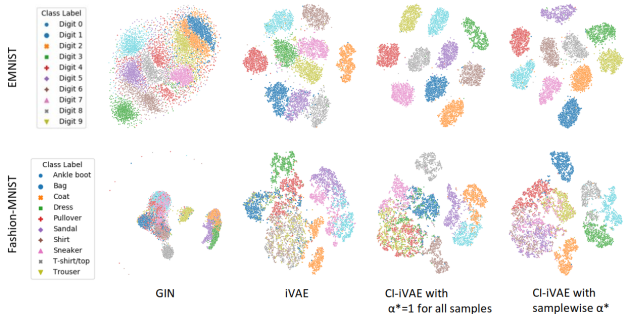


Figure 2. Visualization of the two-dimensional t-SNE (Van der Maaten & Hinton, 2008) embeddings of representations, conditional expectation of latent variables given observations, from various methods on EMNIST and Fashion-MNIST datasets.

$2.3 \times 10^{-27}$  for EMNIST and  $8.8 \times 10^{-25}$  for Fashion-MNIST datasets. When GIN is compared with CI-iVAE with samplewise  $\alpha^*$ , p-values are  $2.1 \times 10^{-25}$  for EMNIST and  $3.1 \times 10^{-48}$  for Fashion-MNIST datasets. CI-iVAE with  $\alpha^* = 1$  for all samples are comparable to or better than CI-iVAE with samplewise  $\alpha^*$ . The p-values are  $1.6 \times 10^{-1}$  for EMNIST and  $6.2 \times 10^{-5}$  for Fashion-MNIST. That is, CI-iVAE is significantly better than iVAE and GIN for extracting covariates-related information from observations, and directly enforcing the inverse relation between encoders and decoders is more effective than using sharper lower bounds in these datasets.

Visualization of t-SNE embeddings is presented in Figure 2. In all datasets, CI-iVAE with samplewise optimal  $\alpha^*$  and CI-iVAE with  $\alpha^* = 1$  yield more separable representations by covariates than GIN and iVAE.

Table 4. Means of prediction performances with standard errors from 5-fold cross-validation. We train support vector regression for age and CBCL scores, and support vector machine for sex and puberty. The representation from our methods outperform that from AE and iVAE baselines. Prediction performances with our representations are comparable to or better than those with raw  $X$ .

INPUT	COVARIATES			
	AGE (MSE ↓)	SEX (ERROR RATE ↓)	PUBERTY (F1 SCORE ↑)	CBCL SCORES (MSE ↓)
$X$	.165 (.012)	.105 (.007)	.531 (.023)	<b>.072</b> (.006)
$q_\phi(z x)$ FROM AE	.336 (.005)	.368 (.006)	.188 (.009)	.135 (.006)
$q_\phi(z x)$ FROM iVAE	.361 (.005)	.479 (.010)	.046 (.005)	.148 (.006)
$q_\phi(z x)$ FROM CI-iVAE WITH $\alpha^* = 1$ FOR ALL SAMPLES	.158 (.018)	.088 (.008)	<b>.592</b> (.022)	.075 (.007)
$q_\phi(z x)$ FROM CI-iVAE WITH SAMPLEWISE OPTIMAL $\alpha^*$	<b>.153</b> (.017)	<b>.086</b> (.009)	.563 (.053)	.073 (.008)

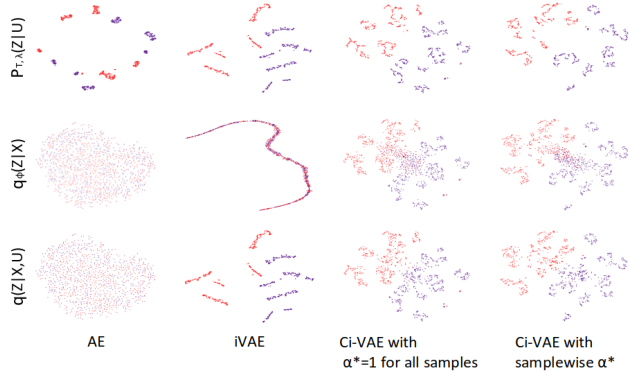


Figure 3. Visualization of the two-dimensional t-SNE embeddings of latent variables from label prior, encoder, and posterior from various methods on the ABCD dataset. Red and blue points indicate female and male, respectively.

#### 4.2.2. APPLICATION TO BRAIN IMAGING DATA FOR PSYCHIATRY RESEARCH

Here we present the application of the CI-iVAE on the Adolescent Brain Cognitive Development (ABCD) study dataset, which is the largest single-cohort prospective longitudinal study of neurodevelopment and children’s mental health in the United States. The ABCD dataset provides resources to address a central scientific question in Psychiatry: can we find the brain imaging representations that are associated with phenotypes. For this purpose, the proposed CI-iVAE is appealing and more efficient in that it incorporates the information in demographics, symptoms, which, by domain knowledge, are associated with brain imaging. In this application, observations are the MRI mean thickness and functional connectivity data from Gordon Atlas (Gordon et al., 2016), and the covariates are interview age, gender, puberty level, and total Child Behavior Checklist (CBCL) scores. We compare CI-iVAE with vanilla AE and iVAE.

The experimental results are presented in Table 4 and Figure 3. Visualization of representations by covariates is provided in Figure 7 in Appendix B.2. We consider prediction performances using representations from various methods to evaluate how much covariate-related information in observa-

tions is extracted from brain measures. We use conditional expectations of encoders,  $q_\phi(z|x)$ , as representations. For the puberty level, we oversample minority classes to balance classes.

According to Table 4, for all covariates, representations from our methods outperform those from AE and iVAE and are comparable to raw observations. CI-iVAE with samplewise optimal  $\alpha^*$  is significantly better than iVAE, p-values for age, sex, puberty level, and CBCL scores are  $1.1 \times 10^{-6}$ ,  $8.4 \times 10^{-10}$ ,  $4.6 \times 10^{-6}$ , and  $3.1 \times 10^{-5}$ , respectively. Thus, our representations extracted from brain measures preserve more covariates-related information than the other methods. There is no significant difference between CI-iVAE with  $\alpha^* = 1$  for all samples and with samplewise optimal  $\alpha^*$ .

Visualization of t-SNE embeddings of latent variables is presented in Figure 3. The result from iVAE demonstrates the limitation of the method. Though the posterior  $q_\phi(z|x, u)$  is very close to the label prior, the encoder  $q_\phi(z|x)$  has little variability, i.e., representations  $Z$  from encoders in iVAE do not contain much information from observations  $X$ . In contrast, the proposed CI-iVAE learns the encoder  $q_\phi(z|x)$  that matches with posterior and prior, and representations are very informative of the covariates  $U$ .

## 5. Discussion

We proposed a new representation learning approach, CI-iVAE, to overcome the limitations of iVAE. Our objective function enforces the inverse relationship between encoders and decoders and is tighter than the ELBO in iVAE under mild conditions. Representations from our methods on various synthetic and real datasets were better than those from existing methods by extracting covariates-associated information in observations. Our work is the first to adapt identifiable generative models to brain imaging. We used pre-processed ROI level summary measures as observations. An interesting future direction is to extract interpretable features from minimally-processed images. Another direction is to apply/develop interpretable machine learning tools creating feature importance scores (Ribeiro et al., 2019; Molnar, 2020; Guidotti et al., 2018) to reveal scientific insights from our representations.



## Acknowledgements

This work is supported by NIMH grant R01 MH124106.

## References

- Bengio, Y., Lamblin, P., Popovici, D., and Larochelle, H. Greedy layer-wise training of deep networks. In *Advances in neural information processing systems*, pp. 153–160, 2007.
- Bengio, Y., Courville, A., and Vincent, P. Representation learning: A review and new perspectives. *IEEE transactions on pattern analysis and machine intelligence*, 35(8): 1798–1828, 2013.
- Bishop, C. M. *Pattern recognition and machine learning*. springer, 2006.
- Cohen, G., Afshar, S., Tapson, J., and Van Schaik, A. Emnist: Extending mnist to handwritten letters. In *2017 International Joint Conference on Neural Networks (IJCNN)*, pp. 2921–2926. IEEE, 2017.
- Dinh, L., Sohl-Dickstein, J., and Bengio, S. Density estimation using real nvp. In *International Conference on Learning Representations*, 2017.
- Goodfellow, I., Pouget-Abadie, J., Mirza, M., Xu, B., Warde-Farley, D., Ozair, S., Courville, A., and Bengio, Y. Generative adversarial nets. In *Advances in neural information processing systems (NeurIPS)*, 2014.
- Gordon, E. M., Laumann, T. O., Adeyemo, B., Huckins, J. F., Kelley, W. M., and Petersen, S. E. Generation and evaluation of a cortical area parcellation from resting-state correlations. *Cerebral cortex*, 26(1):288–303, 2016.
- Guidotti, R., Monreale, A., Ruggieri, S., Turini, F., Gianotti, F., and Pedreschi, D. A survey of methods for explaining black box models. *ACM computing surveys (CSUR)*, 51(5):1–42, 2018.
- Hyvärinen, A. Independent component analysis: recent advances. *Philosophical Transactions of the Royal Society A: Mathematical, Physical and Engineering Sciences*, 371(1984):20110534, 2013.
- Hyvarinen, A. and Morioka, H. Unsupervised feature extraction by time-contrastive learning and nonlinear ica. *Advances in Neural Information Processing Systems*, 29: 3765–3773, 2016.
- Hyvärinen, A. and Oja, E. Independent component analysis: algorithms and applications. *Neural networks*, 13(4-5): 411–430, 2000.
- Hyvärinen, A. and Pajunen, P. Nonlinear independent component analysis: Existence and uniqueness results. *Neural networks*, 12(3):429–439, 1999.
- Hyvarinen, A., Sasaki, H., and Turner, R. Nonlinear ica using auxiliary variables and generalized contrastive learning. In *The 22nd International Conference on Artificial Intelligence and Statistics*, pp. 859–868. PMLR, 2019.
- Ioffe, S. and Szegedy, C. Batch normalization: Accelerating deep network training by reducing internal covariate shift. In *International conference on machine learning*, pp. 448–456. PMLR, 2015.
- Jernigan, T. L., Brown, S. A., and Dowling, G. J. The adolescent brain cognitive development study. *Journal of research on adolescence: the official journal of the Society for Research on Adolescence*, 28(1):154, 2018.
- Jutten, C., Babaie-Zadeh, M., and Karhunen, J. Nonlinear mixtures. In *Handbook of Blind Source Separation*, pp. 549–592. Elsevier, 2010.
- Kameoka, H., Kaneko, T., Tanaka, K., and Hojo, N. Acvaevc: Non-parallel many-to-many voice conversion with auxiliary classifier variational autoencoder. *arXiv preprint arXiv:1808.05092*, 2018.
- Khemakhem, I., Kingma, D., Monti, R., and Hyvarinen, A. Variational autoencoders and nonlinear ica: A unifying framework. In *International Conference on Artificial Intelligence and Statistics*, pp. 2207–2217. PMLR, 2020.
- Kingma, D. P. and Ba, J. Adam: A method for stochastic optimization. *arXiv preprint arXiv:1412.6980*, 2014.
- Kingma, D. P. and Welling, M. Auto-encoding variational bayes. In *Proceedings of the International Conference on Learning Representations (ICLR)*, 2014.
- LeCun, Y. The mnist database of handwritten digits. <http://yann.lecun.com/exdb/mnist/>, 1998.
- LeCun, Y., Bengio, Y., and Hinton, G. Deep learning. *nature*, 521(7553):436–444, 2015.
- Lin, J. Divergence measures based on the shannon entropy. *IEEE Transactions on Information theory*, 37(1):145–151, 1991.
- Liu, J., Pearlson, G., Windemuth, A., Ruano, G., Perrone-Bizzozero, N. I., and Calhoun, V. Combining fmri and snp data to investigate connections between brain function and genetics using parallel ica. *Human brain mapping*, 30(1):241–255, 2009.
- Locatello, F., Bauer, S., Lucic, M., Raetsch, G., Gelly, S., Schölkopf, B., and Bachem, O. Challenging common assumptions in the unsupervised learning of disentangled

- representations. In *international conference on machine learning*, pp. 4114–4124. PMLR, 2019.
- Makhzani, A., Shlens, J., Jaitly, N., Goodfellow, I., and Frey, B. Adversarial autoencoders. In *Proceedings of the International Conference on Learning Representations (ICLR)*, 2015.
- Molnar, C. *Interpretable machine learning*. Lulu. com, 2020.
- Nishiyama, T. A new lower bound for kullback-leibler divergence based on hammersley-chapman-robbins bound. *arXiv preprint arXiv:1907.00288*, 2019.
- Pearlson, G. D., Calhoun, V. D., and Liu, J. An introductory review of parallel independent component analysis (p-ica) and a guide to applying p-ica to genetic data and imaging phenotypes to identify disease-associated biological pathways and systems in common complex disorders. *Frontiers in genetics*, 6:276, 2015.
- Ribeiro, M., Singh, S., and Guestrin, C. Local interpretable model-agnostic explanations (lime): An introduction, 2019.
- Rifai, S., Vincent, P., Muller, X., Glorot, X., and Bengio, Y. Contractive auto-encoders: Explicit invariance during feature extraction. In *Icml*, 2011.
- Schlegl, T., Seeböck, P., Waldstein, S. M., Langs, G., and Schmidt-Erfurth, U. f-anogan: Fast unsupervised anomaly detection with generative adversarial networks. *Medical image analysis*, 54:30–44, 2019.
- Sohn, K., Lee, H., and Yan, X. Learning structured output representation using deep conditional generative models. In *Advances in neural information processing systems*, pp. 3483–3491, 2015.
- Sorrenson, P., Rother, C., and Köthe, U. Disentanglement by nonlinear ica with general incompressible-flow networks (gin). *arXiv preprint arXiv:2001.04872*, 2020.
- Sui, J., He, H., Pearlson, G. D., Adali, T., Kiehl, K. A., Yu, Q., Clark, V. P., Castro, E., White, T., Mueller, B. A., et al. Three-way (n-way) fusion of brain imaging data based on mcca+ jica and its application to discriminating schizophrenia. *NeuroImage*, 66:119–132, 2013.
- Tolstikhin, I., Bousquet, O., Gelly, S., and Schölkopf, B. Wasserstein auto-encoders. In *Proceedings of the International Conference on Learning Representations (ICLR)*, 2018.
- Van der Maaten, L. and Hinton, G. Visualizing data using t-sne. *Journal of machine learning research*, 9(11), 2008.
- Vaserstein, L. N. Markov processes over denumerable products of spaces, describing large systems of automata. *Problemy Peredachi Informatsii*, 5(3):64–72, 1969.
- Vincent, P., Larochelle, H., Bengio, Y., and Manzagol, P.-A. Extracting and composing robust features with denoising autoencoders. In *Proceedings of the 25th international conference on Machine learning*, pp. 1096–1103, 2008.
- Way, G. P., Zietz, M., Rubineti, V., Himmelstein, D. S., and Greene, C. S. Compressing gene expression data using multiple latent space dimensionalities learns complementary biological representations. *Genome biology*, 21:1–27, 2020.
- Xiao, H., Rasul, K., and Vollgraf, R. Fashion-mnist: a novel image dataset for benchmarking machine learning algorithms. *arXiv preprint arXiv:1708.07747*, 2017.
- Xu, B., Wang, N., Chen, T., and Li, M. Empirical evaluation of rectified activations in convolutional network. *arXiv preprint arXiv:1505.00853*, 2015.
- Zeiler, M. D., Krishnan, D., Taylor, G. W., and Fergus, R. Deconvolutional networks. In *2010 IEEE Computer Society Conference on computer vision and pattern recognition*, pp. 2528–2535. IEEE, 2010.
- Zenati, H., Romain, M., Foo, C.-S., Lecouat, B., and Chandrasekhar, V. Adversarially learned anomaly detection. In *2018 IEEE International conference on data mining (ICDM)*, pp. 727–736. IEEE, 2018.
- Zhao, C., Chen, C., He, Z., and Wu, Z. Application of auxiliary classifier wasserstein generative adversarial networks in wireless signal classification of illegal unmanned aerial vehicles. *Applied Sciences*, 8(12):2664, 2018.
- Zhou, D. and Wei, X.-X. Learning identifiable and interpretable latent models of high-dimensional neural activity using pi-vae. In *NeurIPS*, 2020.
- Zong, B., Song, Q., Min, M. R., Cheng, W., Lumezanu, C., Cho, D., and Chen, H. Deep autoencoding gaussian mixture model for unsupervised anomaly detection. In *In Proceedings of the 6th International Conference on Learning Representations*, 2018.

## A. Proofs of Theoretical Results

### A.1. Proofs of Propositions

#### A.1.1. PROOF OF PROPOSITION 1

For any sample  $(x, u)$ ,  $\theta = (f, T, \lambda)$ ,  $\phi$ , and  $\alpha \in [0, 1]$ ,

$$\begin{aligned} \log p_\theta(x|u) &= \log \left( \int \frac{p_\theta(x, z|u)}{\alpha q_\phi(z|x) + (1-\alpha)q_\phi(z|x, u)} \left( \alpha q_\phi(z|x) + (1-\alpha)q_\phi(z|x, u) \right) dz \right) \\ &\geq \int \left( \log \frac{p_\theta(x, z|u)}{\alpha q_\phi(z|x) + (1-\alpha)q_\phi(z|x, u)} \right) \left( \alpha q_\phi(z|x) + (1-\alpha)q_\phi(z|x, u) \right) dz \\ &= \mathbb{E}_{\alpha q_\phi(z|x) + (1-\alpha)q_\phi(z|x, u)} [\log p_\theta(x, z|u) - p_{T, \lambda}(z|u)] - \mathcal{D}_{\text{KL}}(\alpha q_\phi(z|x) + (1-\alpha)q_\phi(z|x, u) \| p_{T, \lambda}(z|u)) \\ &= \mathbb{E}_{\alpha q_\phi(z|x) + (1-\alpha)q_\phi(z|x, u)} \log p_f(x|z) - \mathcal{D}_{\text{KL}}(\alpha q_\phi(z|x) + (1-\alpha)q_\phi(z|x, u) \| p_{T, \lambda}(z|u)) \end{aligned}$$

holds by Jensen's inequality and  $p_\theta(x, z|u) = p_f(x|z)p_{T, \lambda}(z|u)$ .

#### A.1.2. PROOF OF PROPOSITION 2

For any sample  $(x, u)$ ,  $\theta = (f, T, \lambda)$ ,  $\phi$ , and  $\alpha \in [0, 1]$ ,  $\text{ELBO}_{\theta, \phi}(\alpha; x, u)$  can be expressed as

$$\begin{aligned} &\alpha \mathbb{E}_{q_\phi(z|x)} \log p_f(x|z) + (1-\alpha) \mathbb{E}_{q_\phi(z|x, u)} \log p_f(x|z) \\ &- \int \left( \log \frac{\alpha q_\phi(z|x) + (1-\alpha)q_\phi(z|x, u)}{p_{T, \lambda}(z|u)} \right) (\alpha q_\phi(z|x) + (1-\alpha)q_\phi(z|x, u)) dz \\ &= \alpha \left( \text{ELBO}_{\theta, \phi}(1; x, u) + \int \left( \log \frac{q_\phi(z|x)}{p_{T, \lambda}(z|u)} \right) q_\phi(z|x) dz \right) + (1-\alpha) \left( \text{ELBO}_{\theta, \phi}(0; x, u) + \int \left( \log \frac{q_\phi(z|x, u)}{p_{T, \lambda}(z|u)} \right) q_\phi(z|x, u) dz \right) \\ &- \alpha \int \left( \log \frac{\alpha q_\phi(z|x) + (1-\alpha)q_\phi(z|x, u)}{p_{T, \lambda}(z|u)} \right) q_\phi(z|x) dz - (1-\alpha) \int \left( \log \frac{\alpha q_\phi(z|x) + (1-\alpha)q_\phi(z|x, u)}{p_{T, \lambda}(z|u)} \right) q_\phi(z|x, u) dz \\ &= \alpha \text{ELBO}_{\theta, \phi}(1; x, u) + (1-\alpha) \text{ELBO}_{\theta, \phi}(0; x, u) \\ &+ \alpha \mathcal{D}_{\text{KL}}(q_\phi(z|x) \| \alpha q_\phi(z|x) + (1-\alpha)q_\phi(z|x, u)) + (1-\alpha) \mathcal{D}_{\text{KL}}(q_\phi(z|x, u) \| \alpha q_\phi(z|x) + (1-\alpha)q_\phi(z|x, u)) \\ &= \alpha \text{ELBO}_{\theta, \phi}(1; x, u) + (1-\alpha) \text{ELBO}_{\theta, \phi}(0; x, u) + \alpha \mathcal{D}_{\text{skew}}^{1-\alpha}(q_\phi(z|x) \| q_\phi(z|x, u)) + (1-\alpha) \mathcal{D}_{\text{skew}}^\alpha(q_\phi(z|x, u) \| q_\phi(z|x)). \end{aligned}$$

#### A.1.3. PROOF OF PROPOSITION 3

For any sample  $(x, u)$  and  $\alpha \in [0, 1]$ , the first derivative of  $\text{ELBO}_{\theta, \phi}(\alpha; x, u)$  can be expressed as

$$\begin{aligned} \text{ELBO}_{\theta, \phi}^{(1)}(\alpha; x, u) &= \mathbb{E}_{q_\phi(z|x)} \log p_f(x|z) - \mathbb{E}_{q_\phi(z|x, u)} \log p_f(x|z) \\ &- \frac{d}{d\alpha} \int \left( \log \frac{\alpha q_\phi(z|x) + (1-\alpha)q_\phi(z|x, u)}{p_{T, \lambda}(z|u)} \right) (\alpha q_\phi(z|x) + (1-\alpha)q_\phi(z|x, u)) dz \\ &= \left( \text{ELBO}_{\theta, \phi}(1; x, u) + \mathcal{D}_{\text{KL}}(q_\phi(z|x) \| p_{T, \lambda}(z|u)) \right) - \left( \text{ELBO}_{\theta, \phi}(0; x, u) + \mathcal{D}_{\text{KL}}(q_\phi(z|x, u) \| p_{T, \lambda}(z|u)) \right) \\ &- \left[ \int \frac{q_\phi(z|x) - q_\phi(z|x, u)}{\alpha q_\phi(z|x) + (1-\alpha)q_\phi(z|x, u)} (\alpha q_\phi(z|x) + (1-\alpha)q_\phi(z|x, u)) dz \right. \\ &\quad \left. + \int \left( \log \frac{\alpha q_\phi(z|x) + (1-\alpha)q_\phi(z|x, u)}{p_{T, \lambda}(z|u)} \right) (q_\phi(z|x) - q_\phi(z|x, u)) dz \right] \\ &= \text{ELBO}_{\theta, \phi}(1; x, u) - \text{ELBO}_{\theta, \phi}(0; x, u) + \int \left( \log \frac{q_\phi(z|x)}{p_{T, \lambda}(z|u)} \right) q_\phi(z|x) dz - \int \left( \log \frac{q_\phi(z|x, u)}{p_{T, \lambda}(z|u)} \right) q_\phi(z|x, u) dz \\ &- \int \left( \log \frac{\alpha q_\phi(z|x) + (1-\alpha)q_\phi(z|x, u)}{p_{T, \lambda}(z|u)} \right) q_\phi(z|x) dz + \int \left( \log \frac{\alpha q_\phi(z|x) + (1-\alpha)q_\phi(z|x, u)}{p_{T, \lambda}(z|u)} \right) q_\phi(z|x, u) dz \\ &= \text{ELBO}_{\theta, \phi}(1; x, u) - \text{ELBO}_{\theta, \phi}(0; x, u) \\ &+ \mathcal{D}_{\text{KL}}(q_\phi(z|x) \| \alpha q_\phi(z|x) + (1-\alpha)q_\phi(z|x, u)) - \mathcal{D}_{\text{KL}}(q_\phi(z|x, u) \| \alpha q_\phi(z|x) + (1-\alpha)q_\phi(z|x, u)). \end{aligned}$$

With this, the second derivative of  $\text{ELBO}_{\theta,\phi}(\alpha; x, u)$  can be expressed as

$$\begin{aligned}\text{ELBO}_{\theta,\phi}^{(2)}(\alpha; x, u) &= -\frac{d}{d\alpha} \int \left( \log \frac{\alpha q_\phi(z|x) + (1-\alpha)q_\phi(z|x, u)}{p_{T,\lambda}(z|u)} \right) (q_\phi(z|x) - q_\phi(z|x, u)) dz \\ &= -\int \left( \log \frac{q_\phi(z|x) - q_\phi(z|x, u)}{\alpha q_\phi(z|x) + (1-\alpha)q_\phi(z|x, u)} \right) (q_\phi(z|x) - q_\phi(z|x, u)) dz \\ &= -\int \frac{(q_\phi(z|x) - q_\phi(z|x, u))^2}{\alpha q_\phi(z|x) + (1-\alpha)q_\phi(z|x, u)} dz.\end{aligned}$$

Thus,  $\text{ELBO}_{\theta,\phi}^{(2)}(\alpha; x, u) < 0$  for any  $\alpha \in [0, 1]$  if and only if  $q_\phi(z|x) = q_\phi(z|x, u)$  for all  $z$ , which concludes the proof.

## A.2. Lemmas for Theorem 1

In this section, we provide lemmas for Theorem 1 with proofs.

**Lemma 1.** (Equation (18) in Nishiyama (2019)) For any  $t \in [0, 1]$ , real-valued function  $g$ , and probability density functions  $p(z)$  and  $q(z)$ ,

$$\frac{\partial \mathcal{D}_{\text{KL}}(p(z) || (1-t)p(z) + tq(z))}{\partial t} \geq \frac{t(\mathbb{E}_{q(z)}[g(z)] - \mathbb{E}_{p(z)}[g(z)])^2}{t(1-t)(\mathbb{E}_{q(z)}[g(z)] - \mathbb{E}_{p(z)}[g(z)])^2 + (1-t)\text{Var}_{p(z)}[g(z)] + t\text{Var}_{q(z)}[g(z)]}.$$

**Lemma 2.** For any datum  $(x, u)$  and positive number  $\epsilon$ , if there is a function  $g : \mathcal{Z} \rightarrow \mathbb{R}$  satisfying  $\text{SNR}(g) \geq 1/\epsilon$ , then

$$\text{ELBO}_{\theta,\phi}(\alpha; x, u) - \text{ELBO}_{\theta,\phi}(0; x, u) \geq \text{LB}(\alpha, \epsilon, \Delta_{1-0}(x, u))$$

where  $\text{LB}(\alpha, \epsilon, \Delta_{1-0}(x, u)) := \alpha \Delta_{1-0}(x, u) + \alpha \int_\alpha^1 (1-t)/(t(1-t) + \epsilon) dt + (1-\alpha) \int_0^\alpha t/(t(1-t) + \epsilon) dt$ .

*Proof of Lemma A.2.* By Proposition 2,

$$\text{ELBO}_{\theta,\phi}(\alpha; x, u) - \text{ELBO}_{\theta,\phi}(0; x, u) = \alpha \Delta_{1-0}(x, u) + \alpha \mathcal{D}_{\text{KL}}(q_\phi(z|x) || \alpha q_\phi(z|x) + (1-\alpha)q_\phi(z|x, u)) \quad (8)$$

$$+ (1-\alpha) \mathcal{D}_{\text{KL}}(q_\phi(z|x, u) || \alpha q_\phi(z|x) + (1-\alpha)q_\phi(z|x, u)). \quad (9)$$

By substituting  $q_\phi(z|x)$  and  $q_\phi(z|x, u)$  to  $q$  and  $p$  in Lemma 1, respectively, and integrating both sides from 0 to  $\alpha$ , we have

$$\begin{aligned}\mathcal{D}_{\text{KL}}(q_\phi(z|x, u) || \alpha q_\phi(z|x) + (1-\alpha)q_\phi(z|x, u)) \\ \geq \int_0^\alpha \frac{t(\mathbb{E}_{q_\phi(z|x, u)}[g(z)] - \mathbb{E}_{q_\phi(z|x)}[g(z)])^2}{t(1-t)(\mathbb{E}_{q_\phi(z|x, u)}[g(z)] - \mathbb{E}_{q_\phi(z|x)}[g(z)])^2 + (1-t)\text{Var}_{q_\phi(z|x)}[g(z)] + t\text{Var}_{q_\phi(z|x, u)}[g(z)]} dt.\end{aligned}$$

Since  $\text{SNR}(g) \geq 1/\epsilon$ ,

$$\mathcal{D}_{\text{KL}}(q_\phi(z|x, u) || \alpha q_\phi(z|x) + (1-\alpha)q_\phi(z|x, u)) \geq \int_0^\alpha \frac{t}{t(1-t) + \epsilon} dt. \quad (10)$$

In a similar way, we can derive

$$\mathcal{D}_{\text{KL}}(q_\phi(z|x) || \alpha q_\phi(z|x) + (1-\alpha)q_\phi(z|x, u)) \geq \int_\alpha^1 \frac{1-t}{t(1-t) + \epsilon} dt. \quad (11)$$

By (8), (10), and (11), the proof is concluded.  $\square$

**Lemma 3.** The first and second partial derivatives of  $\text{LB}(\alpha, \epsilon, \Delta_{1-0}(x, u))$  w.r.t.  $\alpha$  can be expressed as

$$\frac{\partial \text{LB}(\alpha, \epsilon, \Delta_{1-0}(x, u))}{\partial \alpha} = \Delta_{1-0}(x, u) + \frac{1}{\sqrt{1+4\epsilon}} \log \left| \frac{\alpha - \frac{1+\sqrt{1+4\epsilon}}{2}}{\alpha - \frac{1-\sqrt{1+4\epsilon}}{2}} \right|$$

and

$$\frac{\partial^2 \text{LB}(\alpha, \epsilon, \Delta_{1-0}(x, u))}{\partial \alpha^2} = -\frac{1}{\alpha(1-\alpha) + \epsilon}.$$

Thus,  $\text{LB}(\alpha, \epsilon, \Delta_{1-0}(x, u))$  is strictly concave w.r.t.  $\alpha$  when  $\alpha \in [0, 1]$ .

*Proof of Lemma A.3.* By differentiating  $\text{LB}(\alpha, \epsilon, \Delta_{1-0}(x, u))$  w.r.t.  $\alpha$ , we have

$$\frac{\partial \text{LB}(\alpha, \epsilon, \Delta_{1-0}(x, u))}{\partial \alpha} = \Delta_{1-0}(x, u) + \int_{\alpha}^1 (1-t)/(t(1-t) + \epsilon) dt - \int_0^{\alpha} t/(t(1-t) + \epsilon) dt.$$

Let  $t_+ = \frac{1+\sqrt{1+4\epsilon}}{2}$  and  $t_- = \frac{1-\sqrt{1+4\epsilon}}{2}$ . Since  $\int \frac{t}{t(1-t)+\epsilon} dt = -\frac{t_+}{t_+-t_-} \log|t-t_+| + \frac{t_-}{t_+-t_-} \log|t-t_-| + C$  where  $C$  is the constant of integration and  $\int (1-t)/(t(1-t) + \epsilon) dt = \int t/(t(1-t) + \epsilon) dt$ , we can derive

$$\frac{\partial \text{LB}(\alpha, \epsilon, \Delta_{1-0}(x, u))}{\partial \alpha} = \Delta_{1-0}(x, u) + \frac{1}{\sqrt{1+4\epsilon}} \log \left| \frac{\alpha - \frac{1+\sqrt{1+4\epsilon}}{2}}{\alpha - \frac{1-\sqrt{1+4\epsilon}}{2}} \right|.$$

By differentiating the first derivative w.r.t.  $\alpha$  again, we have  $\frac{\partial^2 \text{LB}(\alpha, \epsilon, \Delta_{1-0}(x, u))}{\partial \alpha^2} = -\frac{1}{\alpha(1-\alpha)+\epsilon}$ .  $\square$

**Lemma 4.** *The maximizer of  $\text{LB}(\alpha, \epsilon, \Delta_{1-0}(x, u))$  over  $\alpha \in [0, 1]$  is  $\alpha_{\text{approx}}^*(\epsilon, \Delta_{1-0}(x, u)) := \frac{1-\sqrt{1+4\epsilon}}{2} + \frac{\sqrt{1+4\epsilon}}{1+e^{-\sqrt{1+4\epsilon}\Delta_{1-0}(x, u)}}$  if and only if  $|\Delta_{1-0}(x, u)| \leq \frac{1}{\sqrt{1+4\epsilon}} \log \frac{(\sqrt{1+4\epsilon}+1)^2}{4\epsilon} = -\log \epsilon + O(\epsilon \log \epsilon)$  as  $\epsilon \rightarrow 0^+$ .*

*Proof of Lemma A.4.* By Lemma 3, the first partial derivative of  $\text{LB}(\alpha, \epsilon, \Delta_{1-0}(x, u))$  w.r.t.  $\alpha$  is zero if and only if  $\alpha = \alpha_{\text{approx}}^*(\epsilon, \Delta_{1-0}(x, u))$ . The solution of  $\alpha_{\text{approx}}^*(\epsilon, \Delta_{1-0}(x, u)) \in [0, 1]$  can be expressed as  $|\Delta_{1-0}(x, u)| \leq \frac{1}{\sqrt{1+4\epsilon}} \log \frac{(\sqrt{1+4\epsilon}+1)^2}{4\epsilon}$ . Next, we prove  $\frac{1}{\sqrt{1+4\epsilon}} \log \frac{(\sqrt{1+4\epsilon}+1)^2}{4\epsilon} = -\log \epsilon + O(\epsilon \log \epsilon)$  as  $\epsilon \rightarrow 0^+$ . We have

$$\left( \frac{1}{\sqrt{1+4\epsilon}} \log \frac{(\sqrt{1+4\epsilon}+1)^2}{4\epsilon} - (-\log \epsilon) \right) \frac{1}{\epsilon \log \epsilon} = \frac{4}{\sqrt{1+4\epsilon}(\sqrt{1+4\epsilon}+1)} - \frac{2}{\sqrt{1+4\epsilon}} \frac{\log 2/(\sqrt{1+4\epsilon}+1)}{\epsilon \log \epsilon}.$$

Here, the first term in RHS converges to 2 as  $\epsilon \rightarrow 0^+$  and, by L'Hospital's rule, the limit of the second term is  $\lim_{\epsilon \rightarrow 0^+} \frac{\log 2/(\sqrt{1+4\epsilon}+1)}{\epsilon \log \epsilon} = \lim_{\epsilon \rightarrow 0^+} \frac{-2/(\sqrt{1+4\epsilon}+1)\sqrt{1+4\epsilon}}{\log \epsilon + 1} = 0$ , which concludes the proof.  $\square$

### A.3. Proof of Theorem 1

Let  $t_+ = \frac{1+\sqrt{1+4\epsilon}}{2}$  and  $t_- = \frac{1-\sqrt{1+4\epsilon}}{2}$ . Since  $\int \frac{t}{t(1-t)+\epsilon} dt = -\frac{t_+}{t_+-t_-} \log|t-t_+| + \frac{t_-}{t_+-t_-} \log|t-t_-| + C$  where  $C$  is the constant of integration and  $\int (1-t)/(t(1-t) + \epsilon) dt = \int t/(t(1-t) + \epsilon) dt$ , we can derive

$$\begin{aligned} \text{LB}(\alpha, \epsilon, \Delta_{1-0}(x, u)) &= \alpha \Delta_{1-0}(x, u) - \frac{\alpha t_+}{t_+-t_-} \log|\alpha-1+t_+| + \frac{\alpha t_-}{t_+-t_-} \log|\alpha-1+t_-| \\ &\quad - \frac{(1-\alpha)t_+}{t_+-t_-} \log|\alpha-t_+| + \frac{(1-\alpha)t_-}{t_+-t_-} \log|\alpha-t_-| + \frac{t_+}{t_+-t_-} \log|t_+| - \frac{t_-}{t_+-t_-} \log|t_-| \\ &= \alpha \Delta_{1-0}(x, u) + \frac{1}{t_+-t_-} (\alpha-t_+) \log|\alpha-t_+| - \frac{1}{t_+-t_-} (\alpha-t_-) \log|\alpha-t_-| \\ &\quad + \frac{t_+}{t_+-t_-} \log|t_+| - \frac{t_-}{t_+-t_-} \log|t_-|. \end{aligned}$$

Here, the last equality is derived by using  $t_+ + t_- = 1$ . By Lemma 4, the maximizer is  $\alpha_{\text{approx}}^*(\epsilon, \Delta_{1-0}(x, u)) = t_- + \sqrt{1+4\epsilon} \sigma(\sqrt{1+4\epsilon} \Delta_{1-0}(x, u))$  where  $\sigma(x) := 1/(1+e^{-x})$  is the sigmoid function, so  $\alpha_{\text{approx}}^*(\epsilon, \Delta_{1-0}(x, u)) - t_+ = -(t_+ - t_-)(1 - \sigma((t_+ - t_-)\Delta_{1-0}(x, u)))$  and  $\alpha_{\text{approx}}^*(\epsilon, \Delta_{1-0}(x, u)) - t_- = (t_+ - t_-)\sigma((t_+ - t_-)\Delta_{1-0}(x, u))$ . Now, substituting these equations and  $(t_+ - t_-)\Delta_{1-0}(x, u) = \log \sigma((t_+ - t_-)\Delta_{1-0}(x, u))/(1 - \sigma((t_+ - t_-)\Delta_{1-0}(x, u)))$

Table 5. A summary of distributions of variables in the simulation study. Examples can be founded at the first column in Figure 1.

LATENT STRUCTURE	VARIABLES		
	COVARIATES ( $U$ )	LATENT VARIABLES GIVEN COVARIATES ( $Z U$ )	OBSERVATIONS GIVEN LATENT VARIABLES ( $X Z$ )
SINE	UNIF( $0, 2\pi$ )	$N((U, 2\sin U)^T, (U/4\pi)I_2)$	$N(\text{REALNVP}(Z), I_{100})$
QUADRATIC	UNIF( $-\pi/2, \pi/2$ )	$N((U, U^2)^T, (2U + \pi)/4\pi I_2)$	$N(\text{REALNVP}(Z), I_{100})$
TWO CIRCLES	UNIF( $-\pi, \pi$ ) $\times$ CAT <sub>2</sub> (0.5, 0.5)	$N((U_2 \cos U_1, U_2 \sin U_1)^T, ( U_1  + \pi)/10\pi I_2)$	$N(\text{REALNVP}(Z), I_{100})$

gives

$$\begin{aligned}
 \text{LB}(\alpha_{\text{approx}}^*(\epsilon, \Delta_{1-0}(x, u)), \epsilon, \Delta_{1-0}(x, u)) &= t_- \Delta_{1-0}(x, u) + \sigma((t_+ - t_-)\Delta_{1-0}(x, u)) \log \frac{\sigma((t_+ - t_-)\Delta_{1-0}(x, u))}{1 - \sigma((t_+ - t_-)\Delta_{1-0}(x, u))} \\
 &\quad - \sigma((t_+ - t_-)\Delta_{1-0}(x, u)) \log \left( (t_+ - t_-)\sigma((t_+ - t_-)\Delta_{1-0}(x, u)) \right) \\
 &\quad - (1 - \sigma((t_+ - t_-)\Delta_{1-0}(x, u))) \log \left( (t_+ - t_-)(1 - \sigma((t_+ - t_-)\Delta_{1-0}(x, u))) \right) \\
 &\quad + \frac{t_+}{t_+ - t_-} \log |t_+| - \frac{t_-}{t_+ - t_-} \log |t_-| \\
 &= t_- \Delta_{1-0}(x, u) - \log(1 - \sigma((t_+ - t_-)\Delta_{1-0}(x, u))) \\
 &\quad + \left( -\log |t_+ - t_-| + \frac{t_+}{t_+ - t_-} \log |t_+| - \frac{t_-}{t_+ - t_-} \log |t_-| \right) \\
 &= \frac{1 + \sqrt{1 + 4\epsilon}}{2} \Delta_{1-0}(x, u) - \log \sigma(\sqrt{1 + 4\epsilon}\Delta_{1-0}(x, u)) \\
 &\quad + \left( -\log(\sqrt{1 + 4\epsilon}) + \frac{1}{2\sqrt{1 + 4\epsilon}} \log \frac{(\sqrt{1 + 4\epsilon} + 1)^2}{4\epsilon} + \frac{1}{2} \log \epsilon \right).
 \end{aligned}$$

Thus,

$$\begin{aligned}
 \sup_{\alpha \in [0, 1]} \text{ELBO}_{\theta, \phi}(\alpha; x, u) - \text{ELBO}_{\theta, \phi}(0; x, u) &\geq \text{LB}(\alpha_{\text{approx}}^*(\epsilon, \Delta_{1-0}(x, u)), \epsilon, \Delta_{1-0}(x, u)) \\
 &= \frac{1 + \sqrt{1 + 4\epsilon}}{2} \Delta_{1-0}(x, u) - \log \sigma(\sqrt{1 + 4\epsilon}\Delta_{1-0}(x, u)) + O(\epsilon \log \epsilon) \text{ as } \epsilon \rightarrow 0^+.
 \end{aligned}$$

Now,  $-\log \sigma(\sqrt{1 + 4\epsilon}\Delta_{1-0}(x, u)) = o(\Delta_{1-0}(x, u))$  as  $\Delta_{1-0}(x, u) \rightarrow \infty$  and  $-\log \sigma(\sqrt{1 + 4\epsilon}\Delta_{1-0}(x, u)) = -\sqrt{1 + 4\epsilon}\Delta_{1-0}(x, u) + o(\Delta_{1-0}(x, u))$  as  $\Delta_{1-0}(x, u) \rightarrow -\infty$  concludes the proof.

## B. Details on Experiments

### B.1. Implementation Details

#### B.1.1. DATASET DESCRIPTION AND EXPERIMENTAL SETTING

We present in Table 6 the three data generation schemes used in the simulation study, which include: 1) distributions of covariates ( $U$ ), 2) conditional distributions of latent variables given covariates ( $Z|U$ ), and 3) conditional distributions of observations given latent variables ( $X|Z$ ). Here, uniform and categorical distributions are denoted by Unif and Cat, respectively, and RealNVP (Dinh et al., 2017) is a flexible and invertible neural network mapping low-dimensional latent variables to high-dimensional observations. As in Zhou & Wei (2020), we use randomly initialized RealNVP networks as ground-truth mixing functions. The sample size is 30,000 and the proportion of training, validation, and test samples are 80%, 10%, and 10%, respectively. The dimension of observations is 100. The number of repeats is 20, and for all datasets and methods, we train five models with different initial weights. All reported results are from models yielding the minimum validation loss and evaluated on the test dataset.

We provide descriptions on real datasets with implementation details.

**EMNIST:** An image dataset consisting of handwritten digits whose data format is the same as MNIST (LeCun, 1998) and has six split types. We use EMNIST split by digits to use images as observations ( $X$ ) and digit labels as covariates ( $U$ ). The official training dataset contains 240,000 images of digits from 0 to 9 in  $28 \times 28$  gray-scale, and the test dataset contains

40,000 images. We randomly split the official training images by 200,000 and 40,000 images to make training and validation datasets for our experiments, and the number of repeats is 20.

**Fashion-MNIST:** An image dataset consisting of fashion-item images with item labels. There are ten classes such as ankle boot, bag, and coat, and we use images as observations ( $X$ ) and item labels as covariates ( $U$ ). The official training and test datasets contain 60,000 and 10,000 images in  $28 \times 28$  gray-scale, respectively, and we randomly split the official training images by 50,000 and 10,000 images to make training and validation datasets. The number of repeats is 20.

**ABCD:** The ABCD study recruited 11,880 children aged 9–10 years (and their parents/guardians) were across 22 sites with 10-year-follow-up. For this analysis, we are using the baseline measures. After list-wise deletion for missing values, the sample size is 5,053, and the dimension of observations is 1,178. We conduct 5-fold cross-validation. For all data splits and methods, we train four models with different initial weights. All reported results are from the model yielding the minimum loss on the validation fold and evaluated on the test fold.

### B.1.2. NETWORK ARCHITECTURES

In all experiments, iVAE, CI-iVAE with  $\alpha^* = 1$  for all samples, and CI-iVAE with samplewise optimal  $\alpha^*$  use the same architectures of the label prior, encoder, and decoder networks for the purpose of fair comparison.

In the simulation study, we modify the official implementation code of pi-VAE. The architectures of label prior and encoder networks are Dense(60)-Tanh-Dense(60)-Tanh-Dense(2) for the sine latent structure and Dense(60)-Tanh-Dense(60)-Tanh-Dense(60)-Tanh-Dense(2) for quadratic and two circles latent structures. As in pi-VAE, we assume  $q(z|x, u) \propto q_\phi(z|x)p_{T,\lambda}(z|u)$ . The  $q(z|x, u)$  is a Gaussian distribution since both label prior and encoder are Gaussian. The means and variances of  $q(z|x, u)$  can be computed with those of label prior and encoder. The architecture of the decoder is the same as the modified GIN used in pi-VAE to guarantee injectivity. We use Adam optimizer (Kingma & Ba, 2014). The number of epochs, batch size, and the learning rate is 100, 300, and  $5 \times 10^{-4}$ , respectively.

In experiments on EMNIST and Fashion-MNIST datasets, we modify the official implementation code of GIN. For GIN, we use the same architecture used in the GIN paper. For iVAE, CI-iVAE with  $\alpha^* = 1$  for all samples, and CI-iVAE with samplewise optimal  $\alpha^*$ , the architecture of encoders is

Conv(32, 3, 1, 1)-BN-LReLU-Conv(64, 4, 2, 1)-BN-LReLU-Conv(128, 4, 2, 1)-BN-LReLU-  
Conv(128, 7, 1, 0)-BN-LReLU-Dense(64),

that of decoders is

ConvTrans(128, 1, 1, 0)-BN-LReLU-ConvTrans(128, 7, 1, 0)-BN-LReLU-ConvTrans(64, 4, 2, 1)-BN-LReLU-  
ConvTrans(32, 4, 2, 1)-BN-LReLU-ConvTrans(1, 3, 1, 1)-Sigmoid,

and that of the label prior is Dense(256)-LReLU-Dense(256)-LReLU-Dense(64). Here, Conv( $f, k, s, p$ ) and ConvTrans( $f, k, s, p$ ) denote the convolution layer and transposed convolution layer (Zeiler et al., 2010), respectively, where  $f, k, s,$  and  $p$  are the number of output channel, kernel size, stride, and padding, respectively. BN denotes the batch normalization layer (Ioffe & Szegedy, 2015), and LReLU denotes the Leaky ReLU activation layer (Xu et al., 2015). The initialized decoders are not injective, but our objective functions encourage them to be injective by enforcing the inverse relation between encoders and decoders. The number of learnable parameters of GIN architectures is 2,620,192, and that of iVAE, CI-iVAE with  $\alpha^*$  for all samples, and CI-iVAE with samplewise optimal  $\alpha^*$  is 2,062,209. We use Adam optimizer. The number of epochs and batch size is 100 and 240, respectively. The learning rate is  $3 \times 10^{-4}$  for the first 50 epochs and is  $3 \times 10^{-5}$  for the remaining epochs.

In the experiment on the ABCD dataset, the architectures of the label prior, encoders, and decoders are Dense(256)-LReLU-Dense(256)-LReLU-Dense(128),

Dense(4096)-BN-LReLU-Dense(4096)-BN-LReLU-Dense(4096)-BN-LReLU-Dense(4096)-BN-LReLU-  
Dense(128)-BN-LReLU-Dense(128),

and

Dense(4096)-LReLU-Dense(4096)-LReLU-Dense(4096)-LReLU-Dense(4096)-LReLU-Dense(128)-LReLU-Dense(128), respectively. We use Adam optimizer. The number of epochs, batch size, and the learning rate is 100 and 64, and  $2 \times 10^{-4}$ , respectively.

Table 6. Means of evaluation metrics with standard errors from various methods and latent structures. The number of repeats is 20.

DATASET	METHOD	EVALUATION METRIC	
		MSE ( $\downarrow$ )	LOG-LIKELIHOOD ( $\uparrow$ )
SINE	iVAE	0.0368 (0.0049)	-131.8387 (1.7467)
	CI-iVAE WITH $\alpha^* = 1$ FOR ALL SAMPLES	0.0083 (0.0003)	-112.9937 (0.8611)
	CI-iVAE WITH SAMPLEWISE $\alpha^*$	<b>0.0072</b> (0.0002)	<b>-111.2823</b> (0.5576)
QUADRATIC	iVAE	0.0156 (0.0004)	-105.4009 (0.1260)
	CI-iVAE WITH $\alpha^* = 1$ FOR ALL SAMPLES	0.0021 (0.0002)	-101.9405 (0.2201)
	CI-iVAE WITH SAMPLEWISE $\alpha^*$	<b>0.0008</b> (0.0001)	<b>-101.0430</b> (0.2420)
TWO CIRCLES	iVAE	0.3428 (0.0354)	-114.9876 (1.2964)
	CI-iVAE WITH $\alpha^* = 1$ FOR ALL SAMPLES	0.0062 (0.0002)	-103.1350 (0.2335)
	CI-iVAE WITH SAMPLEWISE $\alpha^*$	<b>0.0053</b> (0.0002)	<b>-102.9267</b> (0.3198)

 Table 7. Contingency tables to display the number of data by their  $\alpha^*$  computed by grid search (column) and formula (row) on sine latent structure. Correlation coefficients between  $\alpha^*$  by grid search and by formula are presented at the top-left corner.

LATENT STRUCTURE = SINE				
		FORMULA		
CORRELATION COEFFICIENT: 0.99 (0.00)		0	IN-BETWEEN 0 AND 1	1
GRID	0	26.85% (0.18%)	1.88% (0.06%)	0.00% (0.00%)
	IN-BETWEEN 0 AND 1	0.19% (0.01%)	0.14% (0.02%)	0.01% (0.00%)
	1	0.00% (0.00%)	1.99% (0.05%)	68.95% (0.19%)
LATENT STRUCTURE = QUADRATIC				
		FORMULA		
CORRELATION COEFFICIENT: 0.99 (0.00)		0	IN-BETWEEN 0 AND 1	1
GRID	0	30.95% (0.19%)	2.61% (0.06%)	0.00% (0.00%)
	IN-BETWEEN 0 AND 1	0.30% (0.02%)	0.28% (0.02%)	0.04% (0.01%)
	1	0.00% (0.00%)	2.68% (0.08%)	63.14% (0.26%)
LATENT STRUCTURE = TWO CIRCLES				
		FORMULA		
CORRELATION COEFFICIENT: 0.99 (0.00)		0	IN-BETWEEN 0 AND 1	1
GRID	0	36.05% (0.19%)	3.44% (0.08%)	0.00% (0.00%)
	IN-BETWEEN 0 AND 1	0.39% (0.02%)	0.29% (0.02%)	0.02% (0.01%)
	1	0.00% (0.00%)	3.46% (0.08%)	56.36% (0.27%)

## B.2. Further Experimental Results

We present further experimental results on the simulation study in Tables 6 and 7.

According to Table 6, the iVAE is worse than the other two. When iVAE is compared with CI-iVAE with samplewise  $\alpha^*$ , p-values for MSE in sine, quadratic, and two circles latent structures are  $4.5 \times 10^{-6}$ ,  $2.6 \times 10^{-19}$ , and  $5.6 \times 10^{-9}$ , respectively, and for log-likelihood are  $4.0 \times 10^{-10}$ ,  $9.1 \times 10^{-13}$ , and  $1.3 \times 10^{-8}$ , respectively. Moreover, CI-iVAE with samplewise optimal  $\alpha^*$  is better than CI-iVAE with  $\alpha^* = 1$  for all samples. The p-values for MSE in sine, quadratic, and two circles latent structures are  $1.1 \times 10^{-2}$ ,  $3.8 \times 10^{-7}$ , and  $8.6 \times 10^{-3}$ , respectively, and for log-likelihood are  $5.6 \times 10^{-2}$ ,  $6.5 \times 10^{-3}$ , and  $3.0 \times 10^{-1}$ , respectively.

We present contingency tables for samplewise optimal  $\alpha$  computed by grid search (Algorithm 1) and by using approximating formula (Equation (7)) in Table 7. For grid search, we calculate  $\text{ELBO}_{\theta, \phi}(\alpha; x, u)$  for  $\alpha \in \{0, 0.001, \dots, 0.999, 1\}$  and pick the maximizer. For formula, we approximate  $\epsilon$  with  $f(\mathbf{z}) = z_j$  and  $f(\mathbf{z}) = z_j^2$  for  $j = 1, \dots, d_Z$  and calculate  $\alpha_{\text{approx}}^*$ . For all three settings, the correlation coefficients are high, which indicates the consistency of  $\alpha^*$  from the proposed algorithm with theoretical approximation. Moreover,  $\alpha^*$  does not degenerate at 0 or 1, so the proposed CI-iVAE with samplewise optimal  $\alpha^*$  is different from the two ablation cases, iVAE and CI-iVAE with  $\alpha^* = 1$  for all samples.



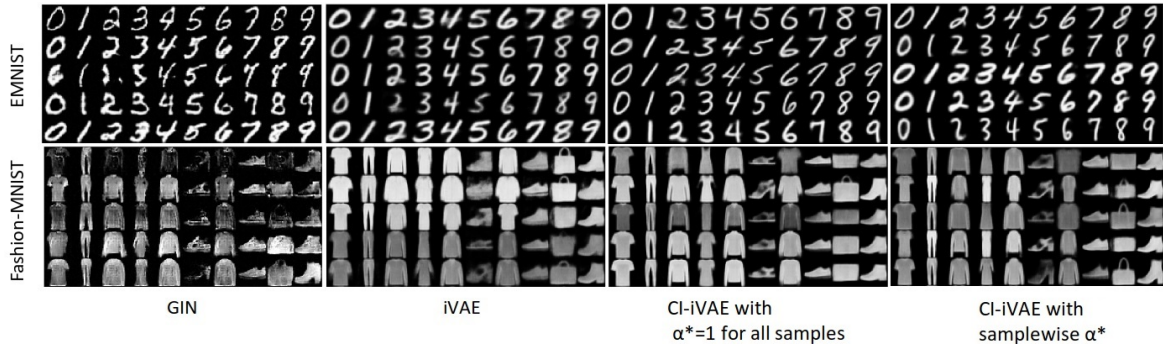


Figure 4. Generation results from various methods on EMNIST and Fashion-MNIST datasets.

Generation results from various methods are presented in Figure 4. For all methods and datasets, samples in each row share random noise to be transformed to latent variables by reparametrization trick. All methods generate visually plausible images, but iVAE-based methods generate relatively smooth results.

Generation results according to attributes having the largest standard deviations are provided in Figures 5 and 6. For all methods, the generated result changes as the value of attributes are changed. In Fashion-MNIST, iVAE-based methods change the contrast of fashion items while GIN does not.

Visualization of representations by covariates is provided in Figure 7. We binarize the covariates to draw plots. For age, sex, puberty, and CBCL scores, red points indicate young age, female, low puberty level, and low CBCL scores, whereas blue points indicate old age, male, high puberty level, and high CBCL scores, respectively. For all covariates, representations from our method show patterns distinguished by covariates, while those from AE and iVAE do not.

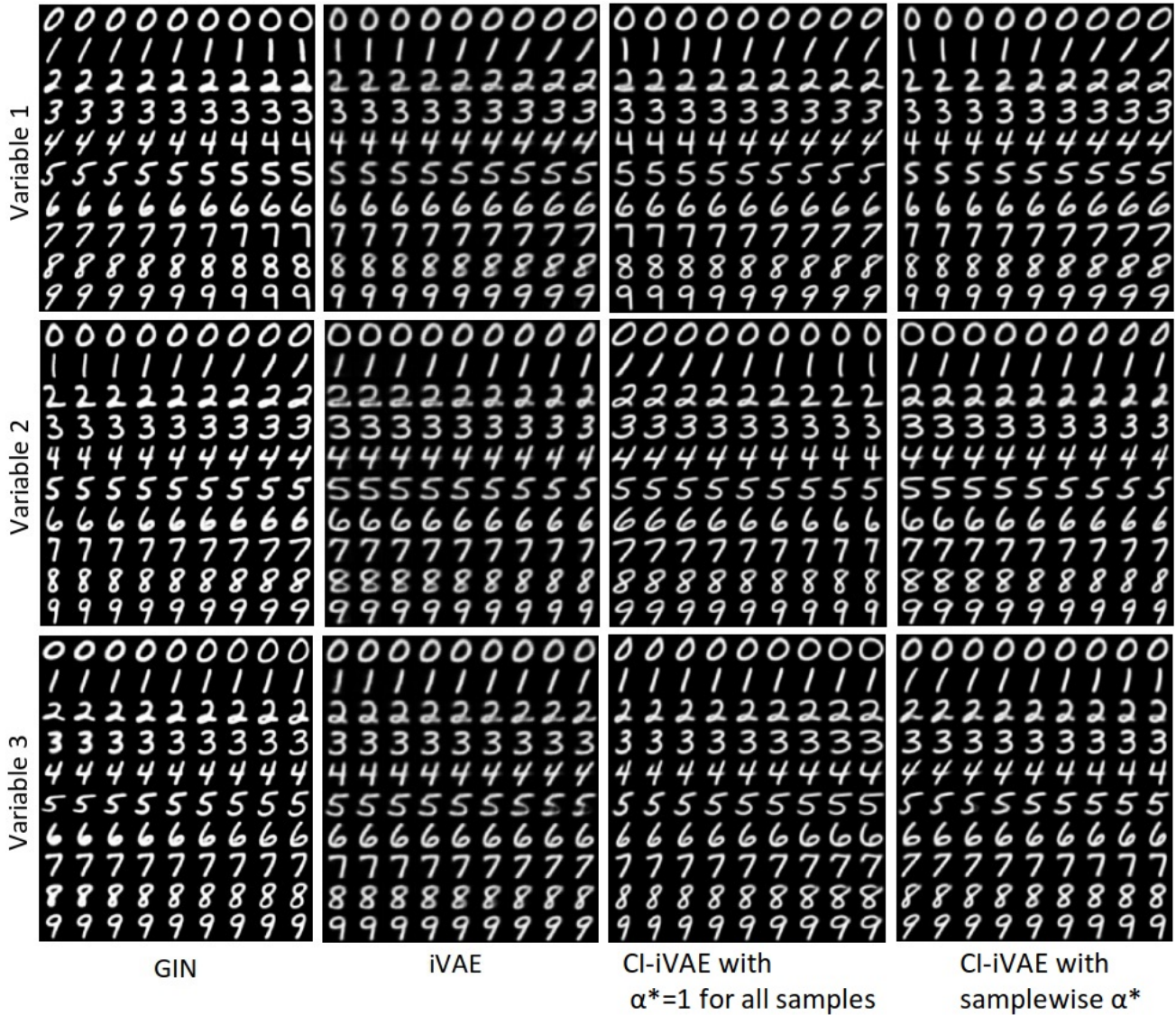


Figure 5. Generation results on EMNIST by varying top three latent attributes having the largest standard deviations. We calculate mean vector of latent variables and controlling the selected attribute from  $-2$  to  $+2$  standard deviations.

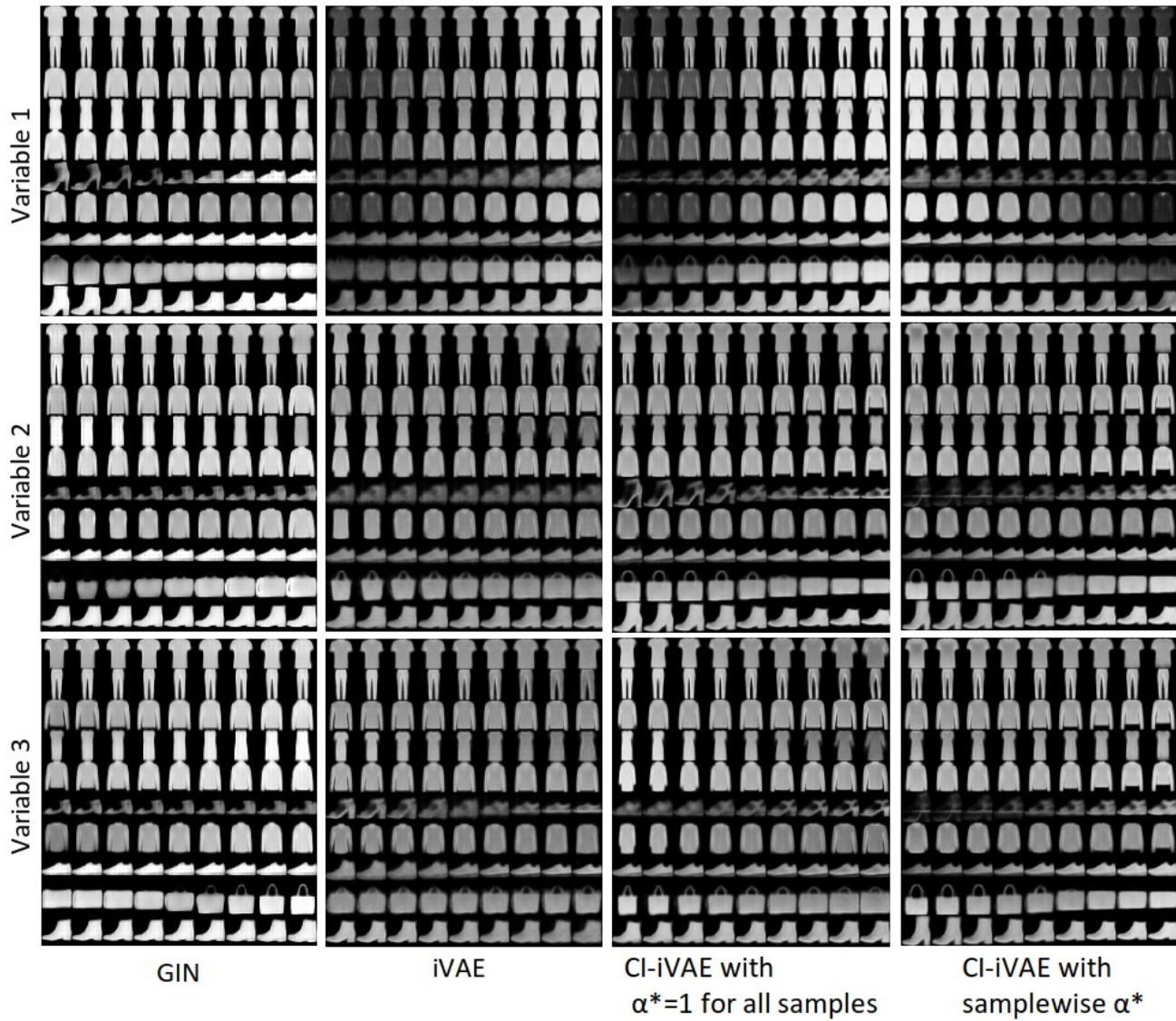


Figure 6. Generation results on Fashion-MNIST by varying top three latent attributes having the largest standard deviations. We calculate mean vector of latent variables and controlling the selected attribute from  $-2$  to  $+2$  standard deviations.

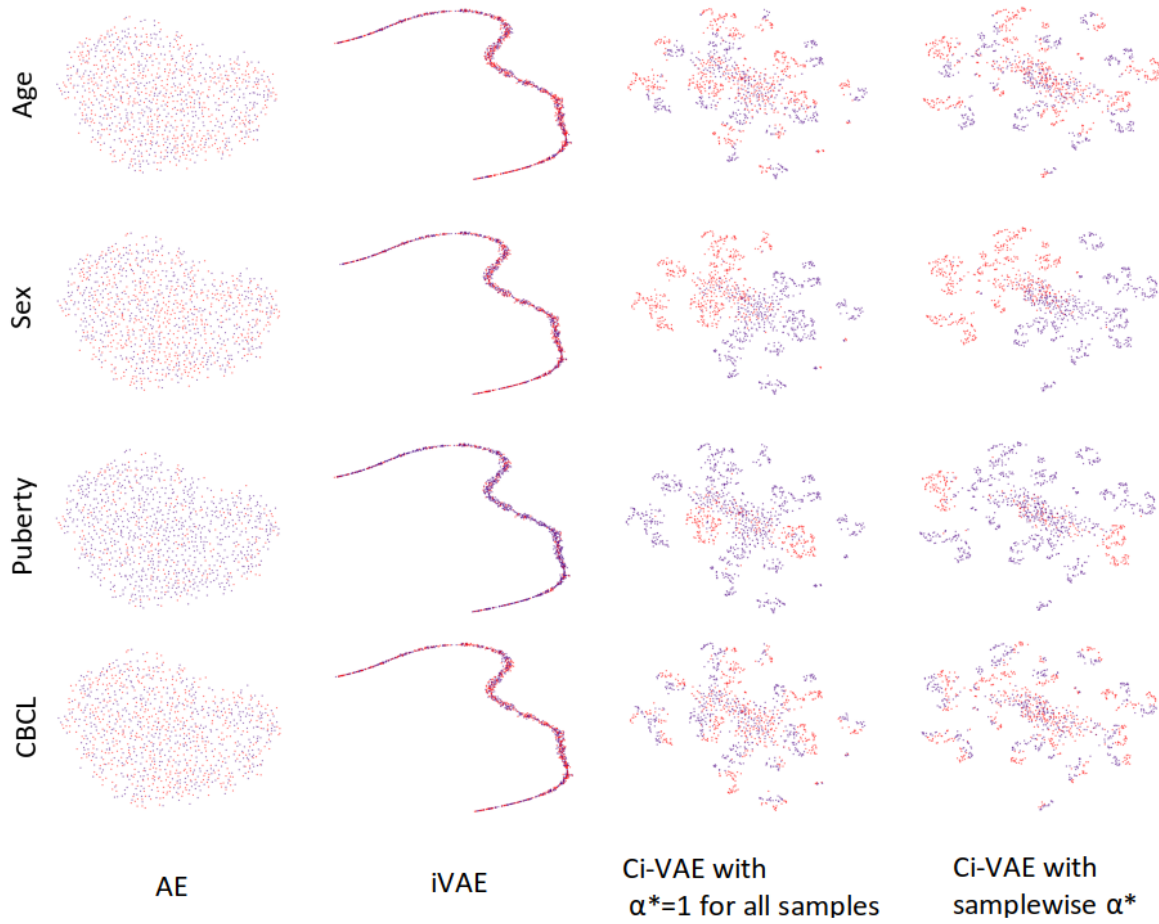


Figure 7. Visualization of the two-dimensional t-SNE embeddings of representations, conditional expectations of encoders  $q_\phi(z|x)$ , from various methods on the ABCD dataset colored by covariates.